



This is to certify that the

thesis entitled


*Attenuation Measurement By
ULTRASONIC Techniques*

presented by

Leenong Li

has been accepted towards fulfillment
of the requirements for

M.S. degree in Electrical Engineering


Major professor

Date 6/19/87



RETURNING MATERIALS:
Place in book drop to
remove this checkout from
your record. FINES will
be charged if book is
returned after the date
stamped below.

SEP 09 1997

ATTENUATION MEASUREMENT BY
ULTRASONIC TECHNIQUES

By

Leenong Li

A THESIS

Submitted to
Michigan State University
in partial fulfillment of the requirements
for the degree

MASTER OF SCIENCE

Department of Electrical Engineering
and System Science

1987

**ATTENUATION MEASUREMENT BY
ULTRASONIC TECHNIQUES**

By

Leenong Li

A THESIS

**Submitted to
Michigan State University
in partial fulfilment of the requirements
for the degree**

MASTER OF SCIENCE

**Department of Electrical Engineering
and System Science**

1987

ABSTRACT

ATTENUATION MEASUREMENT BY

ULTRASONIC TECHNIQUES

By

Leenong Li

This thesis presents ultrasonic measurement techniques for attenuation imaging. The object to be imaged is modeled as consisting of parallel layers of different impedance. Two methods for determining attenuation coefficients are presented. One is to use the impulse response functions. The other is to utilize the ratio of the reflected signals. The theoretical development is verified experimentally by three different measurement configurations. The results of the experiments show that the technique utilizing the ratio of the reflected signals is more accurate than the impulse response technique.

Acknowledgments

I would like to express my sincere appreciation to Dr. Bong Ho and Dr. H. Roland Zapp, my advisors, for their guidance and support. I want to thank Mr. N. T. Wang for offering his FFT program and for many helpful suggestions. I would also like to thank Mr. Tao-shinn Chen for his constant help and encouragement.

Table of Contents

List of Tables	v
List of Figures	vi
Chapter 1 Introduction	1
Chapter 2 Theoretical Considerations	4
2.1 Review of Basic Ultrasound Principles	4
2.2 Ultrasound Reflection from a Layered Model	12
2.3 Determination of Attenuation Coefficient from Impulse Response	15
2.4 Determination of Attenuation Coefficient from Reflected Signals	18
Chapter 3 Experimental Procedures	28
3.1 Experimental Configurations	28
3.2 Data Processing	32
3.3 Experimental Results	50
Chapter 4 Analysis of Experimental Results	64
4.1 Tradeoffs for Finding the Impulse Response Function	64
4.2 Discussion	70
4.3 Conclusion and Suggestion for Future Study	75
Bibliography	78

List of Tables

Table 2.1.1	Approximate values of ultrasonic velocities of various media	5
Table 2.1.2	Characteristic acoustic impedance of various media	10
Table 3.3.1	Result for test object 1 using the impulse response function	63
Table 3.3.2	Result for test object 1 using the signal peak value	63
Table 3.3.3	Result for test object 1 using the signal magnitude sum	63
Table 3.3.4	Result for test object 2	63
Table 3.3.5	Result for test object 3	63
Table 4.2.1	Ratios for simulation data 1	74
Table 4.2.2	Ratios for simulation data 2	74

List of Figures

Figure 2.1.1	Transmission and reflection at an interface	7
Figure 2.2.1	A one dimensional layered structure	13
Figure 2.2.2	First and second order reflection from a layered structure	14
Figure 2.3.1	Bi-directional ultrasonic interrogation	15
Figure 2.4.1	Bi-directional ultrasonic interrogation	19
Figure 2.4.2	A reflected signal waveform	21
Figure 3.1.1	Incident signal processing I	30
Figure 3.1.2	Incident signal recording II	31
Figure 3.1.3	Reflected signal processing I	33
Figure 3.1.4	Reflected signal processing II	34
Figure 3.1.5	Reflected signal processing III	35
Figure 3.2.1	A single layered object for uni-directional attenuation determination	44
Figure 3.2.2	Acoustic transmission and reflection in the single layered object	44
Figure 3.2.3	Sample 1 for the attenuation measurement without knowing the incident signal	48
Figure 3.2.4	Sample 2 for the attenuation measurement without knowing the incident signal	48
Figure 3.3.1	Test object 1 for the bi-directional attenuation measurement	51
Figure 3.3.2	Incident signal for test object 1	51
Figure 3.3.3	Frequency spectrum of the incident signal	51

Figure 3.3.4	Reflected signal from test object 1	52
Figure 3.3.5	Frequency spectrum of the reflected signal	52
Figure 3.3.6	Impulse response function in test 1	53
Figure 3.3.7	Test object 2 for the uni-directional attenuation measurement	55
Figure 3.3.8	Incident signal for test object 2	55
Figure 3.3.9	Frequency spectrum of the incident signal	55
Figure 3.3.10	Impulse response of the incident signal	56
Figure 3.3.11	Reflected signal from the plexi glass/air interface	56
Figure 3.3.12	Frequency spectrum of the reflected signal	57
Figure 3.3.13	Impulse response in test 2	57
Figure 3.3.14	Test object 3 for the attenuation measurement without knowing the incident signal	60
Figure 3.3.15	Incident signal for test 3	60
Figure 3.3.16	Frequency spectrum of the incident signal	60
Figure 3.3.17	Reflected signal in sample 1	61
Figure 3.3.18	Frequency spectrum of the reflected signal in sample 1	61
Figure 3.3.19	Impulse response in sample 1	61
Figure 3.3.20	Reflected signal from sample 2	62
Figure 3.3.21	Frequency spectrum of the reflected signal in sample 2	62
Figure 3.3.22	Impulse response for sample 2	62
Figure 4.1.1	Simulation result for comparison of the impulse response function	66

Figure 4.1.2	Measured result for comparison of the impulse response function	66
Figure 4.1.3	Simulation result without interpolation	68
Figure 4.1.4	Simulation result with interpolation	68
Figure 4.1.5	Measured result without interpolation	69
Figure 4.1.6	Measured result with interpolation	69
Figure 4.1.7	Measured result using correlation	71
Figure 4.2.1	Simulation data 1	73
Figure 4.2.2	Simulation data 2	73

Chapter 1

Introduction

The interaction between ultrasound and even simple biological tissue structures is a complex process. Major factors which describe the propagation of ultrasound in biological material include the density of the material, the sound velocity in the material, the acoustic impedance and the attenuation in the material. By contrast, the propagation of X-rays in tissue is determined solely by the density of the material. Thus, in principle, a considerable amount of information could be extracted from the analysis of the interaction of sound with tissue. This coupled with the noninvasive nature of ultrasound has been its main attraction to biomedical application.

A biomedical ultrasonic imaging system, in general, transmits an acoustic pulse through a test object and receives an echo waveform resulting from the interaction with the object. In transmission systems, the received signal is the deformed pulse resulting from the incident pulse propagating through the object. In reflection systems, the received signal is the waveform resulting from reflections of the incident pulse at the discontinuities inside the object.

Most current ultrasound systems are based on energy detection (or envelope detection) methods and use only the echo amplitude information. A conventional A-scan system displays the amplitude of the echo waveform as a function of acoustic travel time. A conventional B-scan system produces an ultrasonic mapping in which the spot intensity is proportional to the echo intensity. Recently, research has been conducted on how frequency and phase information of the received signal can be used for imaging and tissue characterization. The result produced ultrasonic impediography which allows determination of acoustic impedance along the path of propagation.

This thesis investigates the measurement techniques which can extract the information on acoustic attenuation in addition to acoustical reflection along the path of ultrasound propagation. Attenuation is important from several viewpoints. First, it determines the amount of acoustic energy which can reach structures of interest at various depths in a medium. For example, knowing the attenuation between the surface of a mother's abdomen and the uterine cavity determines the amount of energy reaching the fetus. Second, it is important because part of the propagating energy is permanently converted. Third, attenuation by scattering can result in ultrasonic energy reaching structures not intended to be probed or in production of standing waves, creating peaks and nodes in the spatial distribution

of the ultrasonic energy.

This thesis is organized as follows. First, the basic properties of ultrasound propagation will be briefly reviewed. Second, the basic principles of ultrasonic impediography will be outlined. Third, it will be shown that information sufficient to find out the variation of attenuation along the path of propagation can be extracted by transmitting two ultrasound signals from opposite sides of the test object. For this purpose, the test object is modeled as consisting of parallel layers of different impedances. Fourth, two measurement techniques for determining attenuation variation and impedance profiles will be investigated. Finally, experimental results are presented to show the validity of the theoretical development. The system limitations and suggestion for future study will also be discussed.

Chapter 2

Theoretical Consideration

This chapter provides the necessary theoretical background for the proposed techniques of attenuation and impedance measurement. In the first section, some related ultrasound principles are reviewed. It is followed by the analysis of acoustic reflection from a layered model. With this background we are able to derive a method to determine the acoustic attenuation and impedance profile as will be shown in section 2.3. We propose a simpler and more accurate method in section 2.4.

2.1 Review of Basic Ultrasound Principles

Ultrasonic energy is transported by mechanical vibrations at frequencies above the upper limit of human audibility. The ultrasound consists of a propagating periodic disturbance in the elastic medium, causing the particles of the medium to vibrate about their rest(equilibrium) positions. The vibratory motion of the particles is essential to energy propagation. The transmission through the medium is strongly dependent on the ultrasound frequency and the state of the medium-- gas, liquid, or solid. Table 2.1.1 illustrates that the values of the velocities of longitudinal sound waves in solids are the highest, those in liquids and biological soft tissues lower, and those in gases still lower.

Table 2.1.1 Approximate values of ultrasonic velocities of various media.*

Medium	Sound Velocity(m/s)
Dry air(20 ⁰ C)	343.6
Water(37 ⁰ C)	1524
Amniotic fluid	1530
Brain	1525
Fat	1485
Liver	1570
Muscle	1590
Tendon	1750
Skull bone	3360
Uterus	1625

*From *H.F.Stewart&M.E.Stratmeyer*⁸

In this section, some related properties of ultrasound propagation are reviewed as following.

Sound Velocity

The speed at which ultrasonic vibrations are transmitted through a medium is inversely proportional to the square root of the product of the density and the adiabatic compressibility of the material. The speed of

$$C \propto \sqrt{\frac{B}{\rho}} \quad B: \text{stiffness (modulus)}$$

sound(c), along with frequency(f) determine the wavelength(λ) , from the relationship

$$\lambda = \frac{c}{f} \quad (2.1.1)$$

Knowledge of the speed at which ultrasound is transmitted through a medium is used in the conversion of echo-return time into depth of material being imaged.

Reflection and Transmission at Interfaces

$$Z \equiv \frac{p}{v} \leftarrow \begin{array}{l} \text{pressure} \\ \text{particle} \\ \text{velocity} \end{array}$$

The ratio of the acoustic pressure to the particle velocity in a medium is defined as the specific acoustic impedance for that medium. For plane waves in free field conditions it can be shown that this quantity is equal to the product of the density of the medium(ρ) and the velocity of sound(c) in the medium. Thus the medium characteristic acoustic impedance is:

$$Z = \rho c \quad (2.1.2)$$

When an ultrasonic plane wave meets a boundary between two different media, it may be partially reflected. The ratio of the characteristic impedances of the two media determines the magnitude of the reflection coefficient at the interface. The reflected wave is returned in the negative direction through the incident medium at the same velocity with which it approached the boundary. The transmitted wave continues to

move in a positive direction, but at a velocity corresponding to the propagation velocity in the new medium. Just as in optics, Snell's law for reflection applies, and the angles of incidence and reflection are equal when the wavelength of the ultrasound is small compared to the dimensions and roughness of the reflector as illustrated in Figure 2.1. In Figure 2.1 the subscripts i , r and t refer to the incident, reflected and transmitted waves respectively and 1 and 2 to the first and second media that the ultrasound encounters.

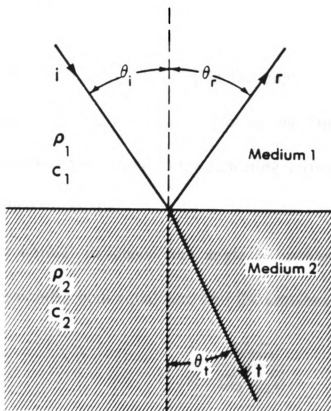


Figure 2.1.1 Transmission and reflection at an interface

The relationship between θ_i and θ_t as given by Snell's law is:

$$C_2 \sin \theta_i = C_1 \sin \theta_r \quad (2.1.3)$$

The equations relating the ratios of the transmitted intensity(I_t) to the incident intensity(I_i) and the reflected intensity(I_r) to the incident intensity(I_i), respectively, are given in the following expressions:

$$\frac{I_t}{I_i} = \frac{(4Z_2Z_1 \cos^2 \theta_i)}{(Z_2 \cos \theta_i + Z_1 \cos \theta_r)^2} \quad (2.1.4)$$

and

$$\frac{I_r}{I_i} = \left[\frac{Z_2 \cos \theta_i - Z_1 \cos \theta_r}{Z_2 \cos \theta_i + Z_1 \cos \theta_r} \right]^2 \quad (2.1.5)$$

where Z_1 and Z_2 are the characteristic acoustic impedances of the media on either side of the interface, θ_i is the angle between the normal to the reflecting surface and the direction of the incident ultrasound, and θ_r is the angle between the normal to the reflecting surface and the direction of the transmitted ultrasound.

For normal incidence, the angle of incidence(θ_i) and the angle of transmission(θ_r) both equal zero and the previous equations become:

$$\frac{I_t}{I_i} = \frac{4Z_2Z_1}{(Z_2 + Z_1)^2} \quad (2.1.6)$$

and

$$\frac{I_r}{I_i} = \left[\frac{Z_2 - Z_1}{Z_2 + Z_1} \right]^2 \quad (2.1.7)$$

These relations can also be expressed in terms of transmitted, reflected, and incident pressures (P_t , P_r , and P_i , respectively), since

$$I = \left(\frac{1}{2}\right) \left(\frac{P^2}{\rho c}\right) \quad (2.1.8)$$

where P is the pressure amplitude we get:

$$\frac{P_t}{P_i} = \frac{2Z_2}{(Z_2 + Z_1)} \quad (2.1.9)$$

and

$$\frac{P_r}{P_i} = \frac{(Z_2 - Z_1)}{(Z_2 + Z_1)} \quad (2.1.10)$$

The reflectivity, or the reflection coefficient, r , is defined as the ratio of pressure reflected to the pressure incident alike the transmissivity, or the transmission coefficient, τ , as the ratio of pressure transmitted to the pressure of the incident wave. Therefore we have the following relationships:

$$r = \frac{P_r}{P_i} = \frac{Z_2 - Z_1}{Z_2 + Z_1} \quad (2.1.11)$$

and

$$\tau = \frac{P_t}{P_i} = \frac{2Z_2}{Z_2 + Z_1} \quad (2.1.12)$$

From equations (2.1.11) and (2.1.12), we can see

$$\tau = 1 + r \quad (2.1.13)$$

Table 2.1.2 lists the characteristic impedances of some biological materials. Analysis of the reflections from a layered model will be discussed in section 2.2.

Table 2.1.2 Characteristic Acoustic Impedances of Various Media.*

Medium	Acoustic Impedance $10^3 \text{kg/(sm}^2\text{)}$
Dry air(20 ⁰ C)	0.45
Water(37 ⁰ C)	1524
Amniotic fluid	1510
Brain	1571
Fat	1366
Liver	1570
Muscle	1685
Tendon	2100
Skull bone	7392
Uterus	1706

***From *H.F.Stewart&M.E.Stratmeyer*⁸**

Attenuation and Absorption

The intensity of a plane progressive ultrasound field can be reduced by interaction with the transmitting medium. Two important sources of

attenuation are scattering and absorption. The interface of each discontinuity within a medium serves as a reflecting surface, the size of which (in relation to the wavelength) determines its effects as a scatterer. Most of the scattered energy diverges from the original direction of propagation and thus the total amount of energy transmitted is reduced. When scattering occurs, the amplitude of the scattered wave is proportional to f^n , where f is the frequency of the ultrasound and n is greater than 1. Thus greater scattering occurs at higher frequencies.

The other significant source of attenuation is absorption, which occurs primarily at the macromolecular level for longitudinal waves. The attenuation due to absorption causes the acoustical energy to be converted to some other form of energy, typically heat.

The acoustic pressure amplitude P_x of a plane progressive ultrasound wave of initial acoustic pressure amplitude P_0 and intensity I_0 at a distance x in any uniform attenuating medium, is described by the relationship:

$$P_x = P_0 e^{-\alpha x} \quad (2.1.14)$$

where e is the base for natural logarithms and α is the amplitude attenuation coefficient of the medium for a given frequency. Since acoustic intensity is proportional to the square of acoustic pressure, this can also be expressed in terms of intensity (I):

$$I_x = I_0 e^{-2\alpha x} \quad (2.1.15)$$

Ultrasonic attenuation in a medium generally increases with increasing frequency in a manner that can be expressed approximately (over a limited frequency range) in the form

$$\alpha = \alpha_0 f^n \quad (2.1.16)$$

where α is the amplitude attenuation coefficient of the medium at a frequency f and α_0 is the attenuation coefficient of the medium at the reference frequency f_0 . For many human tissues and other materials of interest, n has a value between 1 and 2. In sections 2.3 and 2.4, the measurement techniques of attenuation coefficients will be considered in detail.

2.2 Ultrasound Reflections from a Layered Model

The structures of biological tissues and composite materials allow to construct a multilayered model for the purpose of acoustic imaging. The model is shown in Figure 2.2.1.

In the rest of this chapter, the following assumptions are made:

1. Reflections of third and higher order are negligible. This assumption is valid for biological tissues and composite materials in general, since the acoustic impedance variation across media boundaries is not large.

↑
Will be continuous

2. Each layer is homogeneous in acoustical properties (i.e. constant impedance within each layer).

3. The width of the boundaries between layers is small compared to the acoustic wavelength.

0	1	2	...	i	$i+1$...	$N-1$	N
Z_0	Z_1	Z_2	...	Z_i	Z_{i+1}	...	Z_{N-1}	Z_0
α_0	α_1	α_2	...	α_i	α_{i+1}	...	α_{N-1}	α_0
τ_0	τ_1	τ_2	...	τ_i	τ_{i+1}	...	τ_{N-1}	τ_0
	r_1	r_2		r_i	r_{i+1}		r_{N-1}	r_N

Figure 2.2.1 A one-dimensional layered model

where:

Z_i =Acoustic impedance of the i th layer

α_i =Attenuation coefficient of the i th layer in Np/s

τ_i =Time taken for acoustic wave to propagate through the i th layer

r_i =Reflection coefficient at the boundary between (i-1)st and i th layers

The impulse response, $h(t)$, of such a structure consists of N

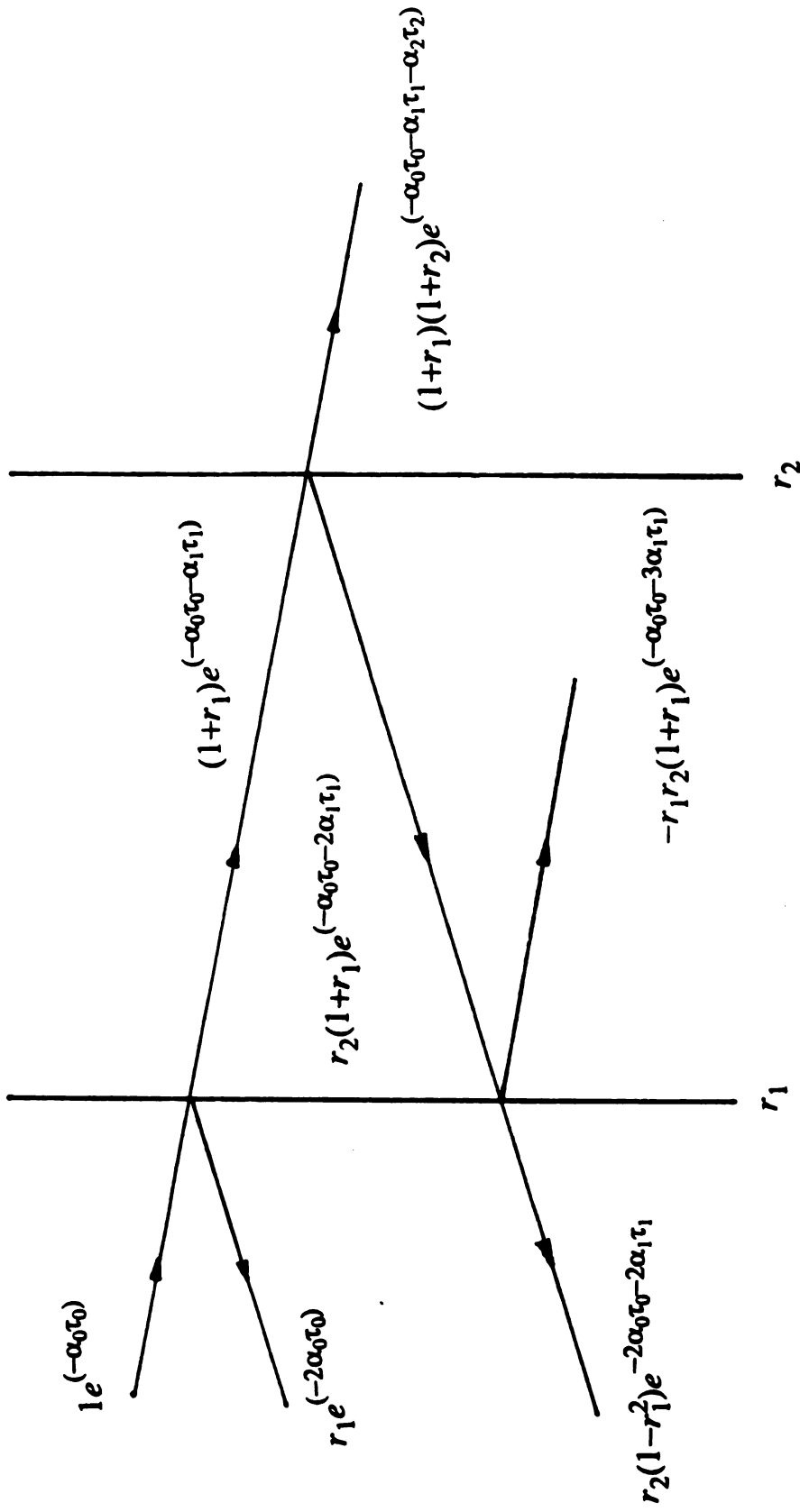


Figure 2.2.2 First and second order reflection from a layered structure

impulses, one for each boundary.

$$h(t) = \sum_{i=1}^N a_i \delta(t - t_i) \quad (2.2.1)$$

where a_i and t_i are the amplitude and delay corresponding to the reflection at the i th interface. Figure 2.2.2 shows the amplitude relationships at each boundary.

In Figure 2.2.2,

$$t_i = \sum_{k=0}^{i-1} 2\tau_k \quad (2.2.2)$$

$2\tau_k$ = round trip delay in k th layer

$$a_i = e^{(-2\alpha_0\tau_0)} r_i \prod_{k=1}^{i-1} (1 - r_k^2) e^{(-2\alpha_k\tau_k)} \quad (2.2.3)$$

$$r_i = \frac{Z_i - Z_{i-1}}{Z_i + Z_{i-1}} \quad (2.2.4)$$

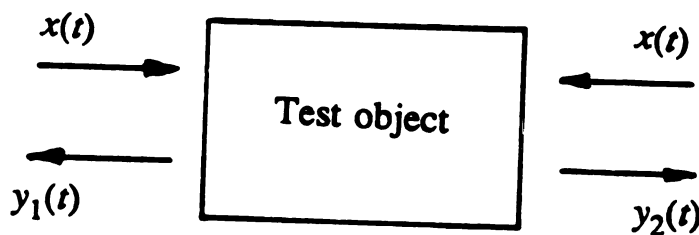


Figure 2.3.1 Bi-directional ultrasonic interrogation

2.3 Determination of Attenuation Coefficients from Impulse Response

The impulse response in equation(2.2.1) contains information on the attenuation coefficient of each layer as well as the reflection coefficient of each boundary. In order to extract the attenuation information, the target is interrogated from the opposite directions as shown in Figure 2.3.1, using an acoustic signal resulting in two impulse response functions. Let the corresponding impulse response functions be $h_1(t)$ and $h_2(t)$. Using the results of section 2.2 and referring to Figure 2.2.2, $h_1(t)$ and $h_2(t)$ can be written as

$$h_1(t) = \sum_{i=1}^N a_i \delta(t - t_i) \quad (2.3.1)$$

where

$$t_i = \sum_{k=0}^i 2\tau_k \quad (2.3.2)$$

$$a_i = e^{(-2\alpha_0\tau_0)} r_i \prod_{k=1}^{i-1} (1 - r_k^2) e^{(-2\alpha_k\tau_k)} \quad (2.3.3)$$

$$r_i = \frac{Z_i - Z_{i-1}}{Z_i + Z_{i+1}} \quad (2.3.4)$$

Similarly,

$$h_2(t) = \sum_{j=1}^N b_j \delta(t - t_j) \quad (2.3.5)$$

where

$$t_j = \sum_{k=j}^N 2\tau_k \quad (2.3.6)$$

$$b_j = -e^{(-2\alpha_j\tau_j)} r_j \prod_{k=j+1}^N (1-r_k^2) e^{(-2\alpha_k\tau_k)} \quad (2.3.7)$$

The minus sign in equation (2.3.7) is due to the fact that the reflection coefficient changes its sign when the incident wave is from the opposite side. The values for a_i and b_j ($i, j=1, 2, \dots, N$) can be read directly from the impulse response functions $h_1(t)$ and $h_2(t)$.

Using equations (2.3.3) and (2.3.7), we have

$$\frac{a_i b_{i+1}}{a_{i+1} b_i} = \frac{r_i}{r_{i+1} (1-r_i^2) e^{(-2\alpha_i\tau_i)}} \frac{r_{i+1}}{r_i (1-r_{i+1}^2) e^{(-2\alpha_i\tau_i)}} \quad (2.3.8)$$

Hence the attenuation coefficient α_i can be determined by:

$$\alpha_i = \frac{1}{4\tau_i} \ln \left[\frac{a_i b_{i+1}}{a_{i+1} b_i} (1-r_i^2)(1-r_{i+1}^2) \right] \quad (2.3.9)$$

where a_i , b_i and τ_i are known. The reflection coefficient r_i can be found as follows:

First, the acoustical properties of the first and the last layers are assumed to be known. This normally is the case because the object is immersed in water. Thus,

$$r_1 = e^{(2\alpha_0\tau_0)} a_1 \quad (2.3.10)$$

$$r_N = -e^{(2\alpha_0\tau_0)} b_N \quad (2.3.11)$$

For the rest of the reflection coefficients $r_i (i=1,2,\dots,N-1)$, let

$$R_i = \frac{r_i^2}{1-r_i^2} \quad (2.3.12)$$

so that,

by Dr. Flo's Note:

$$R_{i+1} = R_i \left[\frac{a_{i+1} b_{i+1}}{a_i b_i} \right] \quad \frac{a_i b_i}{a_{i+1} b_{i+1}} = \frac{r_i^2 (1-r_{i+1}^2)}{(1-r_i^2) r_{i+1}^2} \triangleq \frac{R_i}{R_{i+1}}$$

and

$$r_{i+1} = S_{i+1} \left[\frac{R_{i+1}}{R_{i+1}+1} \right]^{1/2} \quad (2.3.14)$$

where,

$$S_{i+1} = \begin{cases} +1, & \text{if } a_{i+1} > 0 \\ -1, & \text{if } a_{i+1} < 0 \end{cases} \quad (2.3.15)$$

Once all the reflection coefficients are known, the attenuation coefficients α_i can be easily calculated from equation (2.3.9).

2.4 Determination of Attenuation Coefficient from Reflected Signals

In section 2.3, it was shown that the ratio of the magnitude of the impulse response determines both attenuation coefficients and reflection coefficients (equations (2.3.9), (2.3.13) and (2.3.14)). Finding the impulse response in general relies on deconvolution, which involves the inverse Fourier transform of the system spectrum. As will be shown in chapter 4,

because of the existence of noise, frequency band limitations of the FFT as well as other factors, the impulse response obtained through deconvolution is not of the same form as that shown in equation (2.2.1). Thus the magnitudes of the impulse responses used for the calculations of attenuation coefficients have some accuracy limitations.

Since, the deconvolution technique requires multiple Fourier transforms (to determine $X(\omega)$, $Y(\omega)$ and $h(t)$), it is time-consuming and not easily implemented in a small system. A simpler and more accurate alternative to deconvolution is to use the magnitudes of reflected signals to determine the attenuation coefficients and reflection coefficients.

Consider the model described in section 2.3 and shown in Figure 2.4.1.

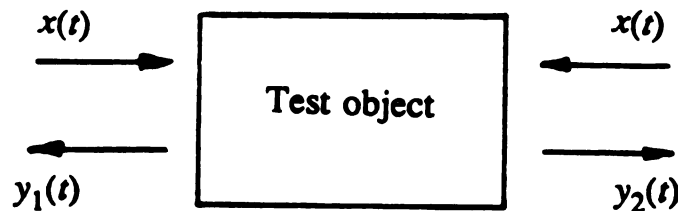


Figure 2.4.1 Bi-directional ultrasonic interrogation

In Figure 2.4.1 $x(t)$ is an incident signal applied to both sides of the object, and $y_1(t)$ and $y_2(t)$ are the reflected signals, respectively. If $h_1(t)$ is

the impulse response for $x(t)$ and $y_1(t)$, $h_2(t)$ for $x(t)$ and $y_2(t)$, then the impulse response $h_1(t)$ from an object with N boundaries consists of N impulses, or

$$h_1(t) = \sum_{i=1}^N a_i \delta(t-t_i) \quad (2.4.1)$$

where a_i is the magnitude of the impulse in the i th interface.

The reflected signal $y_1(t)$ also contains N echoes corresponding to the N interfaces, so that $y_1(t)$ can be expressed as:

$$y_1(t) = \sum_{i=1}^N y_{1i}(t) \quad (2.4.2)$$

where $y_{1i}(t)$ is the i th echo in the reflected signal $y_1(t)$ due to the i th boundary, when interrogated from side 1 of the object. A typical $y_{1i}(t)$ waveforms are shown in Figure 2.4.2.

Because all the $y_{1i}(t)$'s are the reflections of the incident signal $x(t)$, they are of the same frequency as $x(t)$, and the shapes are similar to that of $x(t)$. In other words, all the echoes are copies of $x(t)$ with different proportionality constants.

That is,

$$\frac{x(t)}{y_{11}}(t) = c_0 \quad (2.4.3)$$

and

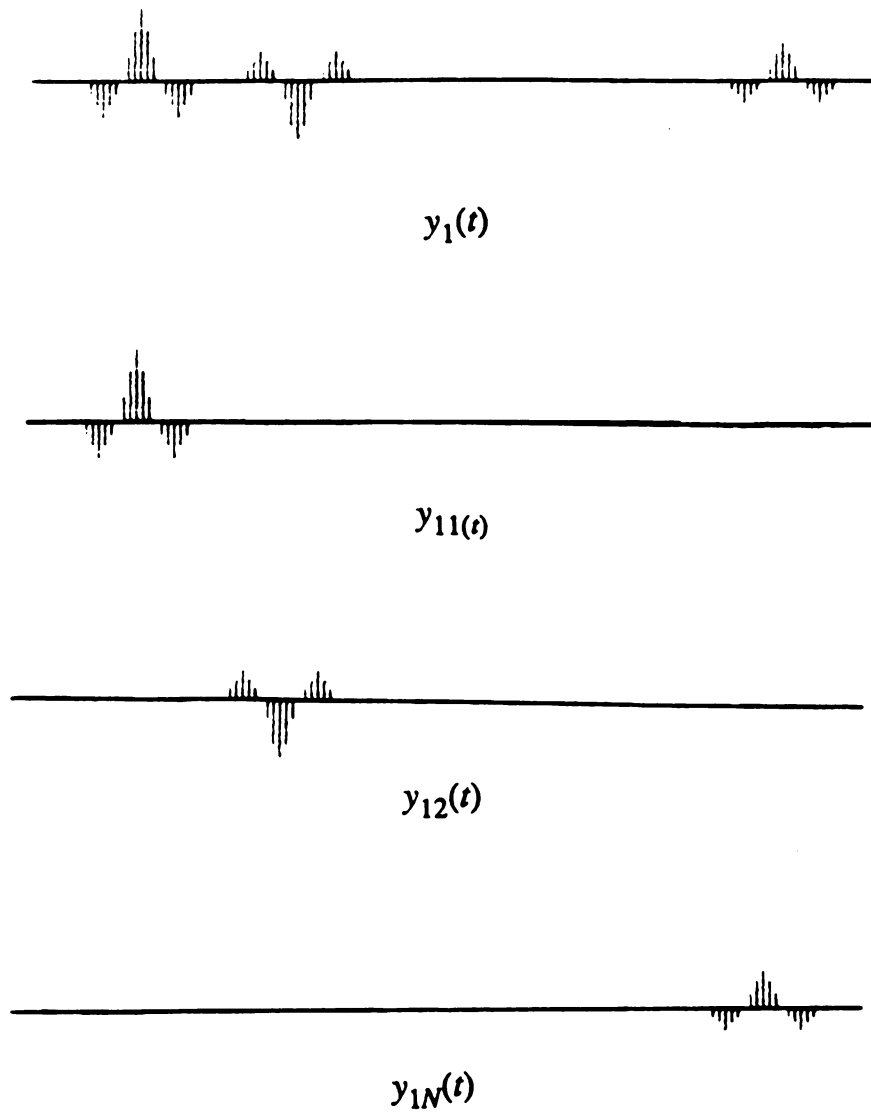


Figure 2.4.2 A reflected signal waveform

$$\frac{y_{1i}(t)}{y_{1(i+1)}} = c_i \quad (2.4.4)$$

where c_0 and c_i are constants.

If $y_{1i}(n)$ and $y_{1(i+1)}(n)$ are the sampled values of $y_{1i}(t)$ and $y_{1(i+1)}(t)$, $x(n)$ is the sampled value of $x(t)$, then by choosing appropriate starting points, we can get

$$\frac{x(n)}{y_{11}(n)} = c_0 \quad (2.4.5)$$

and

$$\frac{y_{1i}(n)}{y_{1(i+1)}(n)} = c_i \quad (2.4.6)$$

for $1 \leq i \leq N$. where N is the number of the boundaries in the object.

Using deconvolution techniques, we can get the impulse response of $y_{1i}(t)$ and $x(t)$ as follows:

With $X(n)$ and $Y_{1i}(n)$ the Fourier transforms of $x(t)$ and $y_{1i}(t)$, respectively,

$$X(k) = \sum_{n=0}^N x(n) e^{-j \frac{2\pi}{N} kn} \quad (2.4.7)$$

$$Y_{1i}(k) = \sum_{n=0}^N y_{1i}(n) e^{-j \frac{2\pi}{N} kn} \quad (2.4.8)$$

where:

$N+1$ = total sampling points of $x(t)$, $y(t)$

$n =$ the n th sampled point of $x(t)$, $y(t)$ at time $t = nT$

$X(k) =$ the k th component of $X(f)$

$Y(k) =$ the k th component of $Y(f)$

The Fourier transform for the impulse response for $y_{1i}(t)$ and $x(t)$ is then given by:

$$H_{1i}(f) = \frac{Y_{1i}(f)}{X(f)} \quad (2.4.9)$$

or

$$H_{1i}(k) = \frac{Y_{1i}(k)}{X(k)} = \frac{\sum_{n=0}^N y_{1i}(n) e^{-j\frac{2\pi}{N}kn}}{\sum_{n=0}^N x(n) e^{-j\frac{2\pi}{N}kn}} \quad (2.4.10)$$

The inverse Fourier transform of $H_{1i}(f)$ provides the impulse response $h_{1i}(n)$:

$$h_{1i}(n) = \sum_{k=0}^N H_{1i}(k) e^{j\frac{2\pi}{N}kn} = \sum_{k=0}^N e^{j\frac{2\pi}{N}kn} \left[\frac{\sum_{n=0}^N y_{1i}(n) e^{-j\frac{2\pi}{N}kn}}{\sum_{n=0}^N x(n) e^{-j\frac{2\pi}{N}kn}} \right] \quad (2.4.11)$$

In a similar manner, the impulse response $h_{(i+1)}(t)$ for $y_{(i+1)}(n)$ and $x(t)$ is given by:

$$h_{1(i+1)}(n) = \sum_{k=0}^N e^{j\frac{2\pi}{N}kn} \left[\frac{\sum_{n=0}^N y_{1(i+1)}(n) e^{-j\frac{2\pi}{N}kn}}{\sum_{n=0}^N x(n) e^{-j\frac{2\pi}{N}kn}} \right] \quad (2.4.12)$$

From equation (2.4.6),

$$x(n) = c_0 y_{11}(n) \quad (2.4.13)$$

$h_{11}(n)$ becomes:

$$h_{11}(n) = \sum_{k=0}^N H_{11}(k) e^{j\frac{2\pi}{N}kn} = \sum_{k=0}^N e^{j\frac{2\pi}{N}kn} \left[\frac{\sum_{n=0}^N y_{11}(n) e^{-j\frac{2\pi}{N}kn}}{\sum_{n=0}^N x(n) e^{-j\frac{2\pi}{N}kn}} \right] \quad (2.4.14)$$

From equation (2.4.3), it is clear that:

$$y_{1i}(n) = c_i y_{1(i+1)}(n) \quad (2.4.15)$$

So that the ratio of $h_{1i}(n)$ to $h_{1(i+1)}(n)$ is:

$$\frac{h_{1i}(n)}{h_{1(i+1)}(n)} = \frac{\sum_{k=0}^N e^{j\frac{2\pi}{N}kn} \left[\frac{\sum_{n=0}^N y_{1i}(n) e^{-j\frac{2\pi}{N}kn}}{\sum_{n=0}^N x(n) e^{-j\frac{2\pi}{N}kn}} \right]}{\sum_{k=0}^N e^{j\frac{2\pi}{N}kn} \left[\frac{\sum_{n=0}^N y_{1(i+1)}(n) e^{-j\frac{2\pi}{N}kn}}{\sum_{n=0}^N x(n) e^{-j\frac{2\pi}{N}kn}} \right]} = c_i \quad (2.4.16)$$

where c_i is the constant determined in equation (2.4.6).

*It has been shown that the ratio of the magnitudes of any two reflected signals is equal to the ratio of the corresponding amplitude impulse responses.

Since the impulse response for the reflected signals and the incident signal is a train of impulses. These impulses must occur at the starting points of the echoes. Thus, the impulses are the first components in $h_{1i}(t)$'s, or $h_{1i}(0)$'s in (2.4.11). The magnitudes a_i and a_{i+1} in equation (2.4.1) become:

$$a_i = h_{1i}(0) \quad (2.4.17)$$

$$a_{i+1} = h_{1(i+1)}(0) \quad (2.4.18)$$

and

$$a_1 = h_{11}(0) = \frac{1}{c_0} \quad (2.4.19)$$

$$\frac{a_i}{a_{i+1}} = \frac{h_{1i}(0)}{h_{1(i+1)}(0)} = c_i \quad (2.4.20)$$

For the opposite side of the model illustrated in Figure 2.4.1, the same conclusions can be drawn.

If $h_2(t)$ is the impulse response for $x(t)$ and $y_2(t)$, then

$$h_2(t) = \sum_{i=1}^N b_i \delta(t - t_i) \quad (2.4.21)$$

and as in equation (2.4.5) and equation (2.4.6);

$$\frac{x(n)}{y_{21}(n)}=d_0 \quad (2.4.22)$$

and

$$\frac{y_{2i}(n)}{y_{2(i+1)}(n)}=d_i \quad (2.4.23)$$

By the procedure shown above:

$$b_N=h_{21}(0)=\frac{1}{d_0} \quad (2.4.24)$$

and

$$\frac{b_i}{b_{(i+1)}}=\frac{h_{2i}(0)}{h_{2(i+1)}(0)}=d_i \quad (2.4.25)$$

where d_i is the constant defined in equation (2.4.23)

Therefore, equations (2.3.9) and (2.3.13) become

$$\alpha_i=\frac{1}{4\tau_i}Ln\left[\frac{a_i b_{i+1}}{a_{i+1} b_i}(1-r_i^2)(1-r_{i+1}^2)\right]=\frac{1}{4\tau_i}Ln\left[\frac{c_i}{d_i}(1-r_i^2)(1-r_{i+1}^2)\right] \quad (2.4.26)$$

$$R_{i+1}=R_i\left[\frac{a_{i+1} b_{i+1}}{a_i b_i}\right]=R_i\left[\frac{1}{c_i d_i}\right] \quad (2.4.27)$$

In the above development, we have shown that the ratio of the magnitudes of the impulse responses can be replaced by the ratio of the *corresponding reflected echoes. This provides a convenient method for determining attenuation coefficients and reflection coefficients. The technique is simple to implement in small systems for on-line imaging appli-

cations. Furthermore, because of the complex numerical calculations and the frequency band limitations of the FFT algorithm in deconvolution, the ratio of the reflected echoes discussed above will provide more accurate results than deconvolution. In chapter 4, it will be shown that for the ideal case, both techniques give the same result. For measured signals, the two techniques give different results, with the results obtained from the ratio of the echoes more reliable.

Chapter 3

Experimental Procedure

The various measurement techniques to verify the theoretical developments in section 2.3 and section 2.4 are discussed in this chapter. Section 3.1 presents the system configurations used in the experimental study. Section 3.2 outlines several data processing procedures to calculate the ultrasonic parameters. The measured data and the experimental results are given in section 3.3.

3.1 Experimental Configurations

In order to calculate the attenuation coefficient and impedance profile, the knowledge of incident signal and reflected signal waveforms is required. The systems used for recording the incident signal and the reflected signals are shown in Figures 3.1.1, 3.1.2, 3.1.3 and 3.1.4. The purpose of these configurations is to provide a wide range comparison of the different measurement techniques. The following subsections explain these configurations.

3.1.1 Sampling Incident Signal Waveform

The system in Figures 3.1.1 and 3.1.2 was used to obtain the incident signal from a lossless acoustic reflection. This was done by observing and

recording the acoustic ultrasound reflection at the air/water interface. Total reflection at the interface was assumed since the acoustic impedance of water is about 3400 times of that of air (refer to Table 2.1.2). The attenuation of ultrasound in water was neglected. A transducer of frequency 2.25 MHz was used. A Panametrics 5050 Pulse Generator/Receiver was employed to generate pulse signals to the transducer and to received the reflected signals. A low energy, intermediate dampen ultrasound signal was used throughout the experimental study.

In Figure 3.1.1, a Tektronix 465 Cathode Ray Oscilloscope was used to display the received signal waveforms. The waveforms were sampled at a 16 MHz sampling rate.

In Figure 3.1.2, the incident signal was sampled by an A/D conversion circuit with a sampling rate of 15MHz. ^{**} The sampled data were sent to a Cromemco Z-2D microcomputer in which a Chebyshev filter with 2.5 MHz passband and 5.0 MHz stopband was implemented. The filtered data were displayed on a monitor and also stored on floppy disks.

The sampled incident signals from either system above were inputted to a Cordata PC400 microcomputer for further processing.

3.1.2 Sampling Reflected Signal Waveforms

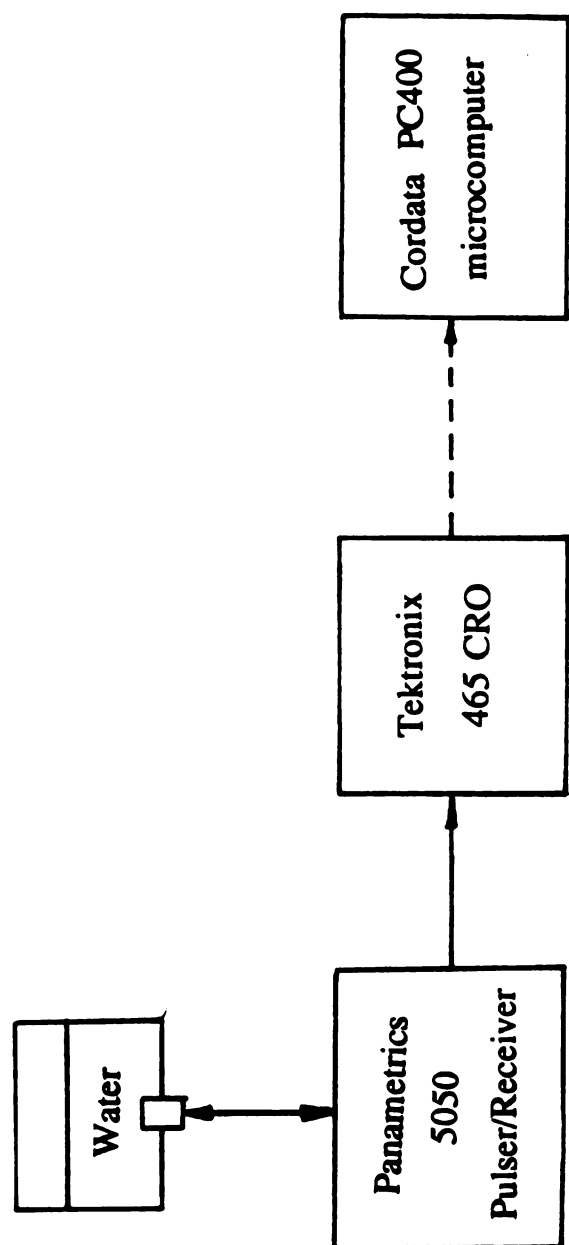


Figure 3.1.1 Incident signal processing I

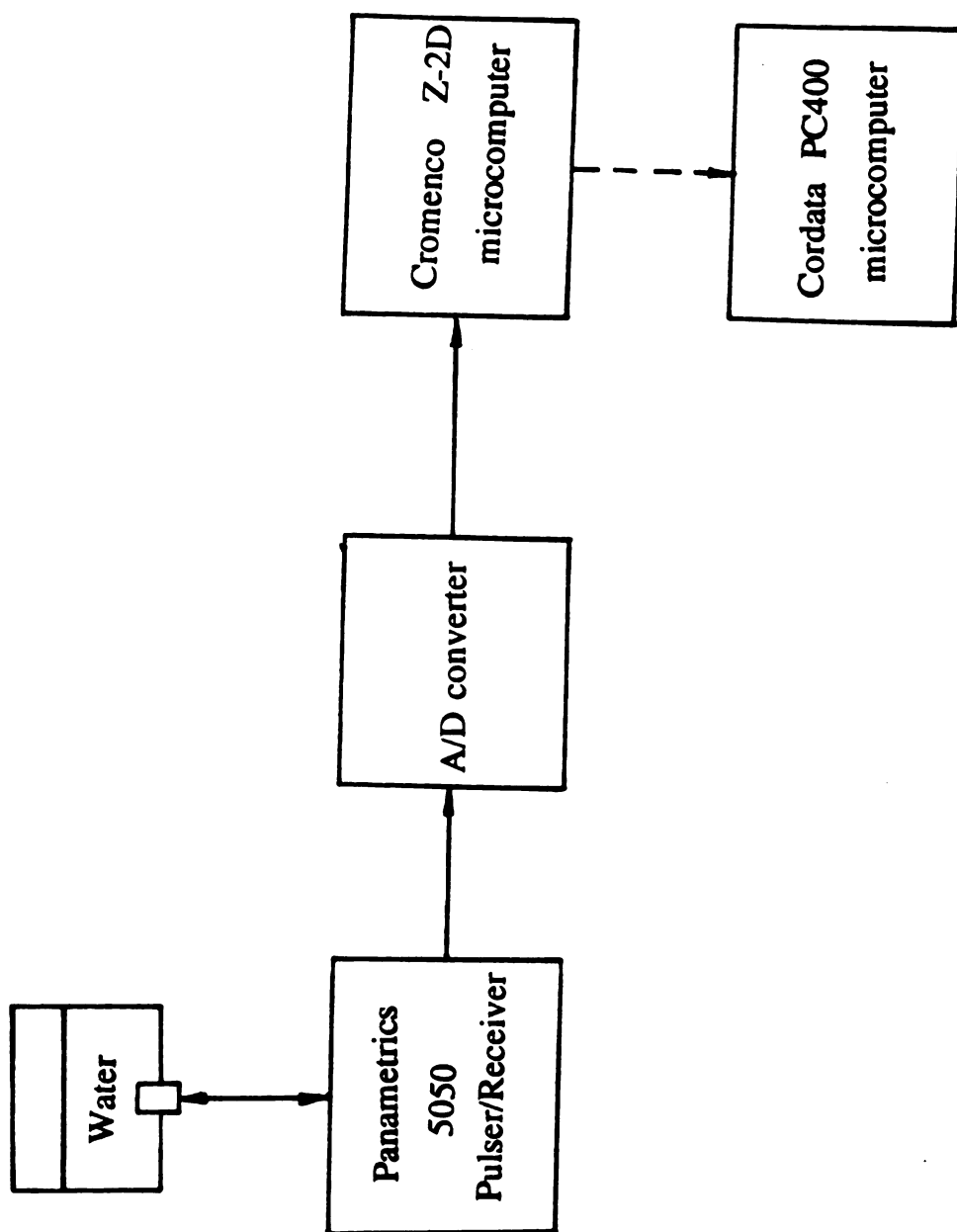


Figure 3.1.2 Incident signal recording II

The reflected signals from a object under test can be obtained in a similar manner, that is to transmit an ultrasound signal to the object and then to receive the echoes from the object. Figure 3.1.3 shows the configuration using an oscilloscope to receive the reflected signal waveforms. The operation and the parameters were the same as those for the incident signal case in Figure 3.1.1. The same ultrasound signal was applied to both sides of the object for the bi-directional interrogation calculation discussed in section 2.3.

The signal in Figure 3.1.4 was applied to the A/D conversion circuit, similar to the signal in Figure 3.1.2. Both side A and side B were exposed the same ultrasound signal, similar to the case in Figure 3.1.3. Figure 3.1.5 shows still another setup for the measurement methods that will be discussed in section 3.2. In this arrangement, only one side of the object is needed for the ultrasound signal.

3.2 Data Processing

Based on the theoretical development in sections 2.3 and 2.4, three different procedures of the attenuation calculation are presented in this section. They are discussed in the following three subsections.

3.2.1 Bi-directional Interrogation

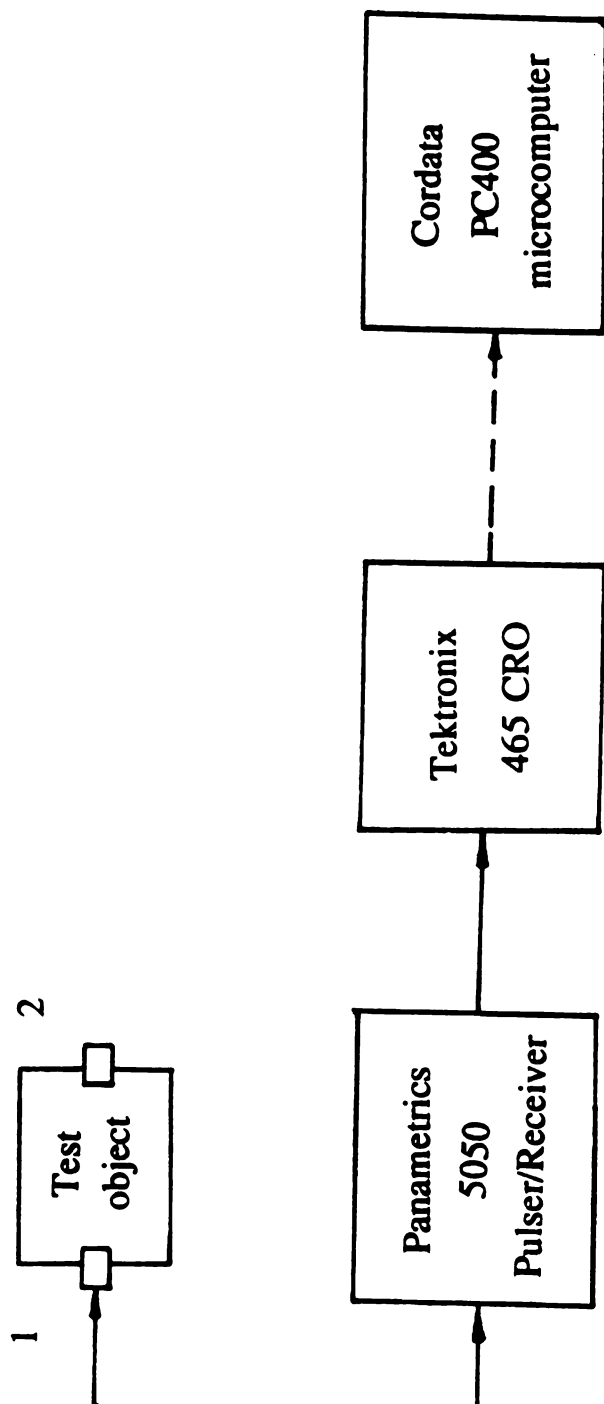


Figure 3.1.3 Reflected signal processing I

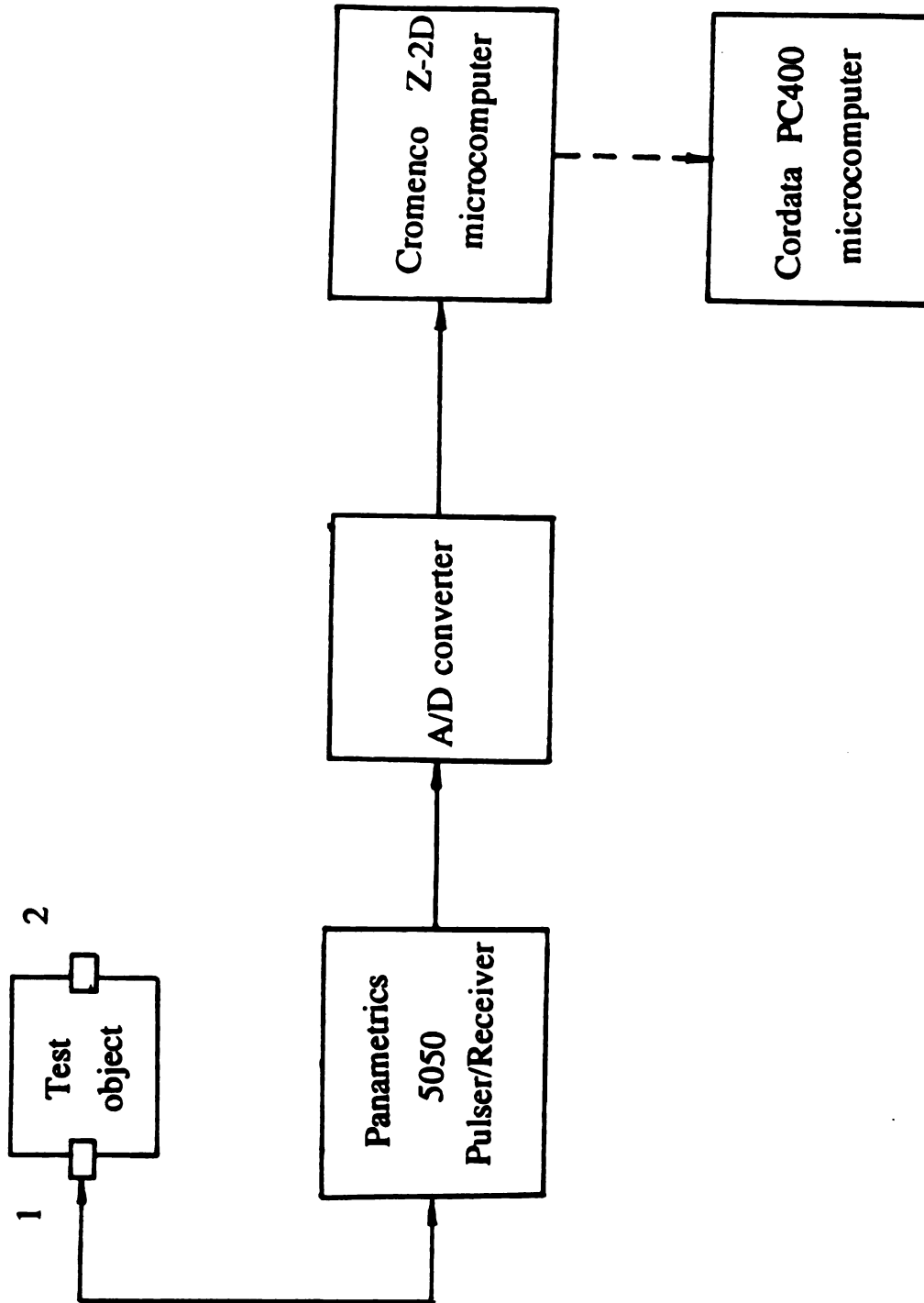


Figure 3.1.4 Reflected signal processing II

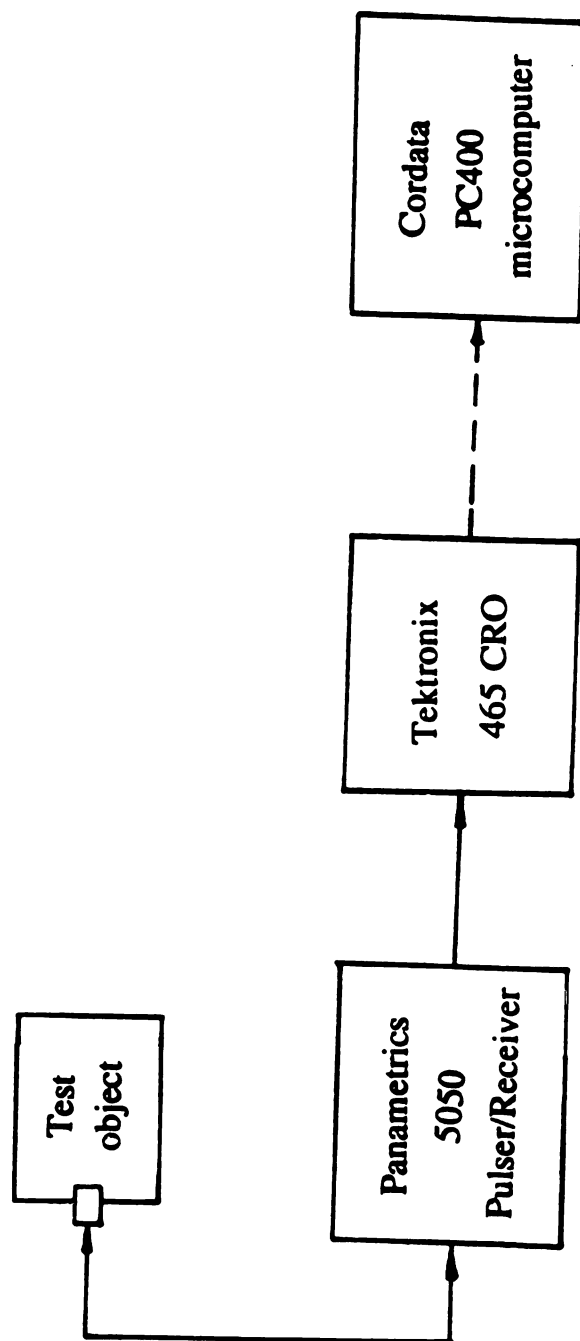


Figure 3.1.5 Reflected signal processing III

The experimental setup involved in this method is shown in Figures 3.1.1, 3.1.2, 3.1.3 and 3.1.4. Two calculation methods for attenuation and for impedance are described as follows.

I) Using the Impulse Response Function

1. An estimate the acoustic impulse response of the object when it is interrogated from either side is achieved as follows:

First obtain the sampled incident signal $x(n)$ and the sampled reflected signals $y_1(n)$ and $y_2(n)$ from side 1 and side 2 of the target. Then transform $x(n)$, $y_1(n)$ and $y_2(n)$ into frequency domain to obtain $X(f)$, $Y_1(f)$ and $Y_2(f)$, respectively.

The reflection transfer function, $H(f)$, is obtained from both sides of the object as:

$$H_1(f) = \frac{Y_1(f)}{X(f)} \quad (3.2.1)$$

and

$$H_2(f) = Y_2 \frac{(f)}{X(f)} \quad (3.2.2)$$

Finally, the impulse response functions are calculated as:

$$h_1(t) = F^{-1}(H_1(f)) \quad (3.2.3)$$

and

$$h_2(t) = F^{-1}(H_2(f)) \quad (3.2.4)$$

where F^{-1} is the inverse Fourier transform operator.

2. Obtain the impedance profile and attenuation variation using the impulse response function

This was done by applying equation (2.3.9) through equation (2.3.15), assuming the attenuation of ultrasound in water to be negligible. Equation (2.3.9) through equation (2.3.15) can be rewritten as:

$$r_1 = a_1 \quad (3.2.5)$$

$$r_N = -b_N \quad (3.2.6)$$

For $i=1,2,\dots,N-2$,

$$R_i = \frac{r_i^2}{1-r_i^2} \quad (3.2.7)$$

$$R_{i+1} = R_i \frac{a_{i+1}b_{i+1}}{a_i b_i} \quad (3.2.8)$$

$$r_{i+1} = S_{i+1} \left[\frac{R_{i+1}}{1+R_{i+1}} \right]^{\frac{1}{2}} \quad (3.2.9)$$

where

$$S_{i+1} = \begin{cases} +1, & \text{if } a_{i+1} > 0 \\ -1, & \text{if } a_{i+1} < 0 \end{cases} \quad (3.2.10)$$

$$\alpha_i = \frac{1}{4\tau_i} \text{Ln} \left[\frac{a_i b_{i+1}}{a_{i+1} b_i} (1-r_i^2)(1-r_{i+1}^2) \right] \quad (3.2.11)$$

and

$$\frac{Z_i}{Z_0} = \frac{1+r_i}{1-r_i} \frac{Z_{i-1}}{Z_0} \quad (3.2.12)$$

The notation used above is defined as follows:

N = number of interfaces

r_i = reflection coefficient from the i th interface

a_i = magnitude of the reflected impulse due to the i th interface, when interrogated from side 1

b_i = magnitude of the reflected impulse due to the i th interface, when interrogated from side 2

α_i = attenuation coefficient in the layer bounded by i th and $(i+1)$ st interface

Z_i = acoustic impedance of the layer between i th and $(i-1)$ st interface

$e^{(-2\alpha_i\tau_i)}$ = loss factor-- the total loss when the signal propagates forward and backward in the layer between i th and $(i+1)$ st interface

Equations (3.2.7) through (3.2.12), together with either equation (3.2.5) or equation (3.2.6). are sufficient to determine the impedance profile and the attenuation variation.

II) Using the Magnitude of the Reflected Signals As discussed in section 2.4, the ratio of the magnitudes of the sampled signals can also deter-

mine the attenuation and impedance. This method does not require knowledge of the impulse response. Therefore there is no Fourier transform technique involved in this method.

The procedure is as follows:

1. Estimate the ratios of the sampled signals

Let $x(n)$ be the sampled incident signal, $y_1(n)$ and $y_2(n)$ the sampled reflected signals when interrogated from side 1 and side 2 of the object, respectively. Thus $y_1(n)$ and $y_2(n)$ can be written as:

$$y_1(n) = \sum_{i=1}^N y_{1i}(n) \quad (3.2.13)$$

$$y_2(n) = \sum_{i=1}^N y_{2i}(n) \quad (3.2.14)$$

where $y_{1i}(n)$ and $y_{2i}(n)$ are the sampled echoes from the i th interface of the object, when interrogated from side 1 and side 2 of the object, respectively.

In Figure 2.4.2, it was shown that the $y_{1i}(n)$'s and $y_{2i}(n)$ have the same length of time duration if appropriately chosen. This is important for the following derivation.

Two methods were used to determine the ratio of the signal magnitudes as follows:

a) Ratio of the summation of the echo magnitudes

The magnitudes of the sampled signals were summed as:

$$x = \sum_{n=0}^m |x(n)| \quad (3.2.15)$$

$$y_{1i} = \sum_{n=0}^m |y_{1i}(n)| \quad (3.2.16)$$

$$y_{1(i+1)} = \sum_{n=0}^m |y_{1(i+1)}(n)| \quad (3.2.17)$$

$$y_{2i} = \sum_{n=0}^m |y_{2i}(n)| \quad (3.2.18)$$

$$y_{2(i+1)} = \sum_{n=0}^m |y_{2(i+1)}(n)| \quad (3.2.19)$$

The ratios in equations (2.4.5), (2.4.18), (2.4.20) and (2.4.23) were determined by:

$$\frac{x(n)}{y_{11}}(n) = c_0 = \frac{\sum_{n=0}^m |x(n)|}{\sum_{n=0}^m |y_{11}(n)|} \quad (3.2.20)$$

$$\frac{a_i}{a_{i+1}} = c_i = \frac{y_{1i}(n)}{y_{1(i+1)}(n)} = \frac{\sum_{n=0}^m |y_{1i}(n)|}{\sum_{n=0}^m |y_{1(i+1)}(n)|} \quad (3.2.21)$$

$$\frac{x(n)}{y_{21}}(n) = d_0 = \frac{\sum_{n=0}^m |x(n)|}{\sum_{n=0}^m |y_{21}(n)|} \quad (3.2.22)$$

$$\frac{b_i}{b_{i+1}} = d_i = y_{2i} \frac{(n)}{y_2} (i+1) = \frac{\sum_{n=0}^m |y_{2i}(n)|}{\sum_{n=0}^m |y_{2(i+1)}(n)|} \quad (3.2.23)$$

b) Ratios of the peak values of the sampled signals

The peak values of the sampled signals were also used to estimate the ratios. They are:

$$\frac{x(n)}{y_{11}}(n) = c_0 = \frac{\max|x(n)|}{\max|y_{11}(n)|} \quad (3.2.24)$$

for $0 \leq n \leq m$

$$\frac{a_i}{a_{i+1}} = c_i = y_{1i} \frac{(n)}{y_{1(i+1)}}(n) = \frac{\max|y_{1i}(n)|}{y_{1(i+1)}(n)} \quad (3.2.25)$$

for $0 \leq n \leq m$

$$\frac{x(n)}{y_{21}}(n) = d_0 = \frac{\max|x(n)|}{\max|y_{21}(n)|} \quad (3.2.26)$$

$$\frac{b_i}{b_{i+1}} = d_i = y_{2i} \frac{(n)}{y_{2(i+1)}}(n) = \frac{\max|y_{2i}(n)|}{\max|y_{2(i+1)}(n)|} \quad (3.2.27)$$

where $m+1$ is the number of sampled points.

2. Calculate the impedance and attenuation using the ratios of the signal magnitudes

The reflection coefficients for the first and the last boundaries(interface 1 and interface N in Figure 2.2.1) were determined using the result of section 2.4. For side 1 of the object,

$$r_1 = a_1 = h_{11}(0) = \frac{1}{c_0} \quad (3.2.28)$$

where c_0 is determined by either equation (3.2.20) or equation (3.2.24).

For side 2 of the object,

$$r_N = -b_N = -h_{21}(0) = -\frac{1}{d_0} \quad (3.2.29)$$

where d_0 is determined by either equation (3.2.22) or equation (3.2.26).

For interface 2 through interface $N-2$,

$$R_i = \frac{r_i^2}{1-r_i^2} \quad (3.2.30)$$

$$R_{i+1} = R_i \frac{a_{i+1}}{a_i} \frac{b_{i+1}}{B_i} = R_i \frac{1}{c_i} \frac{1}{d_i} \quad (3.2.31)$$

$$r_{i+1} = S_{i+1} \left[\frac{R_{i+1}}{1+R_{i+1}} \right] \quad (3.2.32)$$

where S_{i+1} is defined in equation (3.2.17)

$$\alpha_i = \frac{1}{4\tau_i} \ln \left[\frac{a_i}{a_{i+1}} \frac{b_{i+1}}{b_i} (1-r_i^2)(1-r_{i+1}^2) \right] = \frac{1}{4\tau_i} \ln \left[c_i \frac{1}{d_i} (1-r_i^2)(1-r_{i+1}^2) \right] \quad (3.2.33)$$

and

$$\frac{Z_i}{Z_0} = \frac{1+r_i}{1-r_i} \frac{Z_{i-1}}{Z_0} \quad (3.2.34)$$

All notation used here are consistent with those in equation (3.2.6) through equation (3.2.13).

Similar to the impulse response method, equations (3.2.30) through (3.2.34), together with either equation (3.2.28) or equation (3.2.29), are sufficient for the attenuation and impedance calculations.

3.2.2. Uni-Directional Attenuation Knowing the Incident Signal

This method can determine the attenuation coefficient of a single layer structure. It requires transmission of an ultrasonic signal into one side of the test object. The reflection coefficient must be known in order to calculate the attenuation coefficient. The systems used are shown in Figures 3.1.1, 3.1.2 and 3.1.5. The test object is shown in Figure 3.2.1. Assuming complete acoustic reflection at the material/air interface and the attenuation of ultrasound signal in water to be negligible, the response of the object to an impulse is shown in Figure 3.2.2. The following notation is used in Figure 3.2.2:

a_0 = the impulse response of the incident signal the experimental

a_1 = impulse response from the first interface

a_2 = impulse response from the second interface

r_1 = reflection coefficient from the water/material interface

r_2 = reflection coefficient from the material/air interface; which for total reflection gives $r_2=1$

Z_0 = impedance of water

Z_1 = impedance of the test material

Z_2 = impedance of air

α_1 = attenuation coefficient of the test material

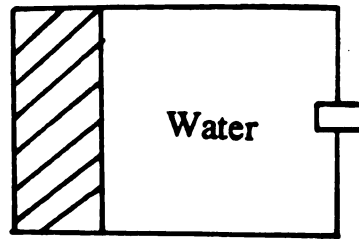


Figure 3.2.1 A single layered object

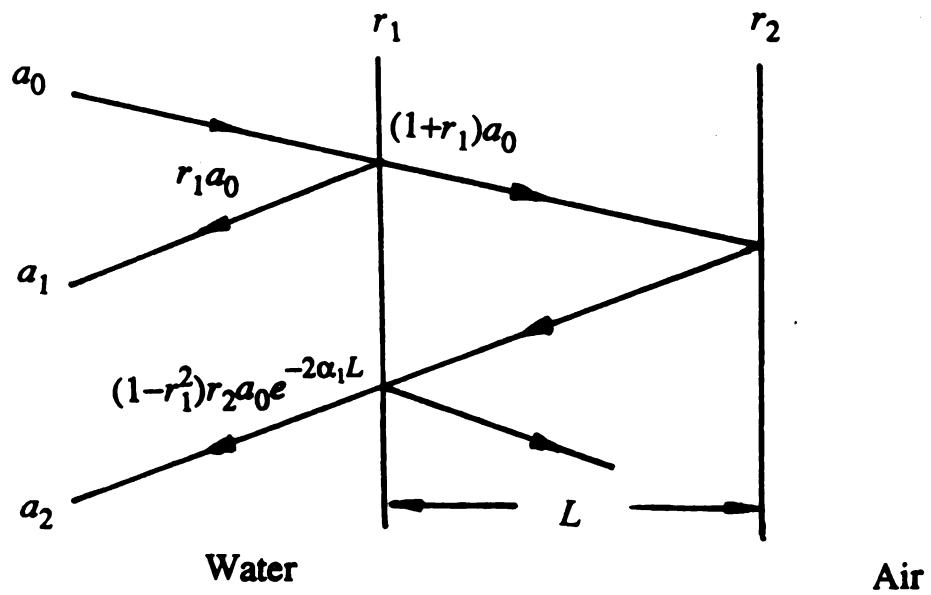


Figure 3.2.2 Acoustic transmission and reflection in the single layered object

L = thickness of the material along the transmission axis

From Figure 3.2.2, it is clear that:

$$a_2 = (1 - r_1^2) r_2 e^{-2\alpha_1 L} \quad (3.2.35)$$

The attenuation coefficient α_1 is therefore:

$$\alpha_1 = \frac{1}{2l} \ln \left[(1 - r_1^2) r_2 \frac{a_0}{a_2} \right] \quad (3.2.36)$$

The ratio $\frac{a_0}{a_2}$ in the equation above can be either the ratio of the impulse response or the ratio of the signal magnitudes, as discussed in subsection 3.2.1.

In equation (3.2.36), the reflection coefficient at the water/material interface, r_1 , needs to be obtained by other means. experimentally, two methods were employed. They are:

a) Obtain r_1 from an impedance calculation.

This is accomplished using the the relationship between impedance and reflection coefficient as shown in equation (2.1.11), which for case here, is:

$$r_1 = \frac{Z_1 - Z_0}{Z_1 + Z_0} \quad (3.2.37)$$

where the variables were defined in Figure 3.2.2. Z_1 and Z_0 are determined as follows:

From equation (2.1.2),

$$Z_1 = \rho_1 c_1 \quad (3.2.38)$$

where: ρ_1 = density of the test material

c_1 = velocity of sound in the material

ρ_1 was calculated by measuring the volume and the weight of the test object. c_1 was obtained by measuring the travel time of the distance in the . Z_0 , impedance of water, was found in published data (Table 2.1.2).

b) Obtain r_1 from a signal waveform

From Figure 3.2.2, the relationship:

$$a_1 = r_1 a_0 \quad (3.2.39)$$

provides the desired reflection coefficient:

$$r_1 = \frac{a_1}{a_0} \quad (3.2.40)$$

Again, $\frac{a_1}{a_0}$ can either be the ratio of the impulse response or the ratio of the signal magnitudes.

Once the reflection coefficient r_1 is determined, the attenuation coefficient α_1 of the material can be calculated from equation (3.2.36).

3.2.3 Uni-directional Attenuation Determination without Knowing the Incident Signal

The method outlined here is similar to the one in the previous subsection. It requires two different thickness samples of the test material. Knowledge of the incident signal is immaterial as long as the same incident signal applied to both samples. Figure 3.1.5 shows the system configuration for this measurement method.

The acoustic reflection and transmission relationship for the two samples are shown in Figures 3.2.3 and 3.2.4.

In Figure 3.2.3, the following notation is used:

a_0 = incident impulse applied to each sample

a_{11} = impulse response from the first boundary of sample 1

a_{12} = impulse response from the second boundary of sample 1

r_1 = reflection coefficient at the water/material interface

α_1 = attenuation coefficient of the test material

L_1 = thickness of sample 1

In Figure 3.2.4, the following notation is used:

a_0 = incident impulse applied to each sample

a_{21} = impulse response from the first boundary of sample 2

a_{22} = impulse response from the second boundary of sample 2

r_2 = reflection coefficient at the material/air interface

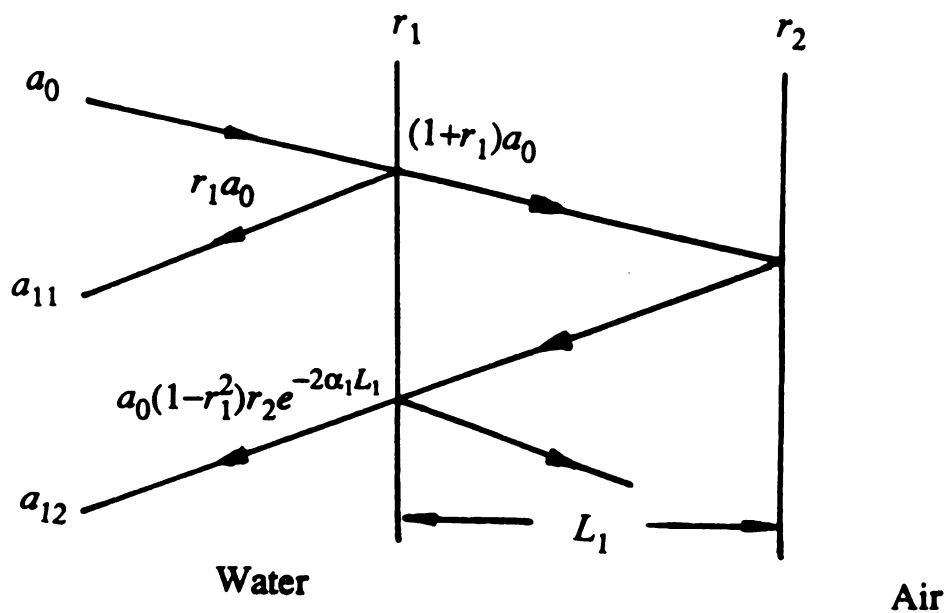


Figure 3.2.3 Sample 1

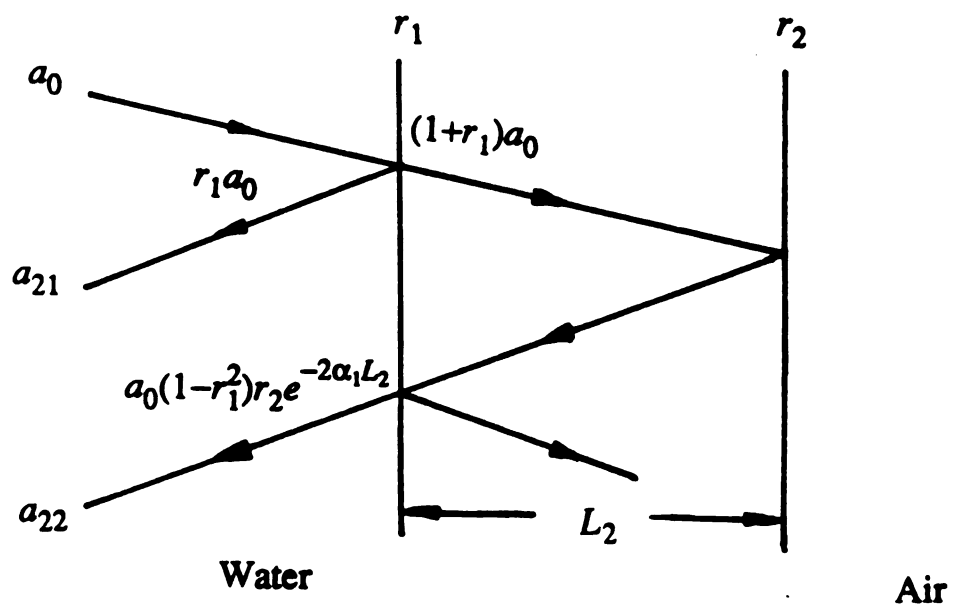


Figure 3.2.4 Sample 2

α_1 = attenuation coefficient of the test material

L_2 = thickness of sample 2

From an analysis similar to subsection 3.2.2, the transmission and reflection coefficients are given by:

$$a_{12} = a_0(1-r_1^2)r_2e^{-2\alpha_1L_1} \quad (3.2.41)$$

and

$$a_{22} = a_0(1-r_1^2)r_2e^{-2\alpha_1L_2} \quad (3.2.42)$$

Which give the ratio:

$$\frac{a_{12}}{a_{22}} = \frac{a_0(1-r_1^2)r_2e^{-2\alpha_1L_1}}{a_0(1-r_1^2)r_2e^{-2\alpha_1L_2}} = e^{2\alpha_1(L_2-L_1)}. \quad (3.2.43)$$

Thus,

$$\alpha_1 = \frac{1}{2(L_2-L_1)} \ln \left[\frac{a_{12}}{a_{22}} \right] \quad (3.2.44)$$

The attenuation coefficient α_1 can be obtained without relying on knowledge of the incident signal or the acoustic reflection. As pointed previously, the ratio $\frac{a_{12}}{a_{22}}$ in equation (3.2.44) can be the impulse response or the ratio of the reflected signals.

Three different measurement techniques for attenuation variation have been described. The first method introduced, bi-directional ultrasound

interrogation, is the most practical one since it can determine the attenuation and impedance of a multilayered material. However, it is the most complex in terms of calculations and measurements. The remaining two methods are fairly simple but apply to only single layered material. This limits their usefulness. The technique described in subsection 3.2.3 is the most accurate because it does not rely on assumptions and uses less measurement data. Thus it provides a useful laboratory verification.

3.3 Experimental Results

The experiments were selected to verify the validity of the measurement methods outlined in section 3.2. A test material was investigated under the different measurement configurations.

3.3.1 Results from the Bi-directional Ultrasound Interrogation

The model used in the experiment is shown in Figure 3.3.1. It is a single layer structure--an acrylic cast(plexi glass). The incident signal and its frequency spectrum are shown in Figures 3.3.2 and 3.3.3. Since the model is a symmetrical structure, it was interrogated only from one side. The corresponding reflected signal is shown in Figure 3.3.4. The frequency spectrum of the reflected signal is shown in Figure 3.3.5. The impulse response obtained is shown in Figure 3.3.6.

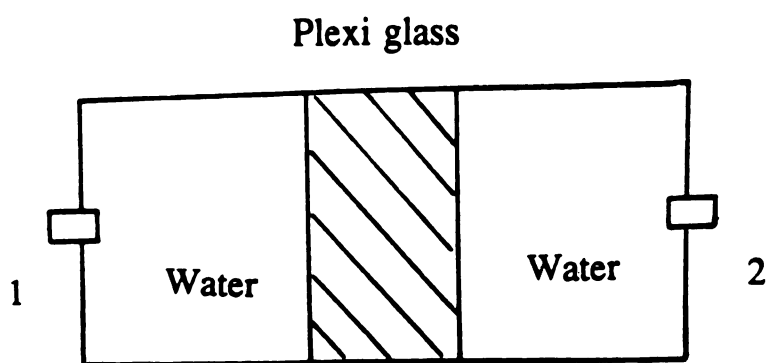


Figure 3.3.1 Test object 1

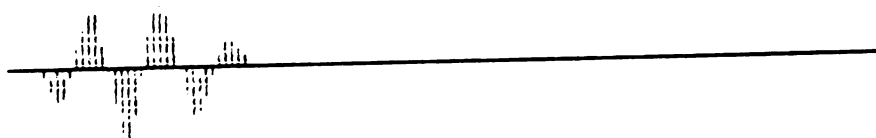


Figure 3.3.2 Incident signal for test object 1

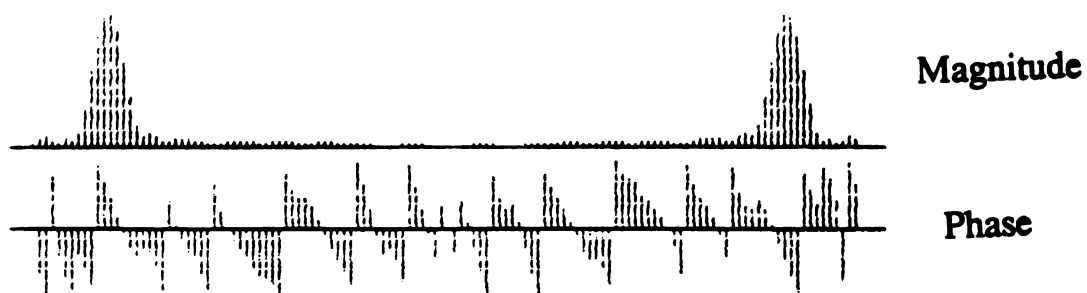


Figure 3.3.3 Frequency spectrum of the incident signal

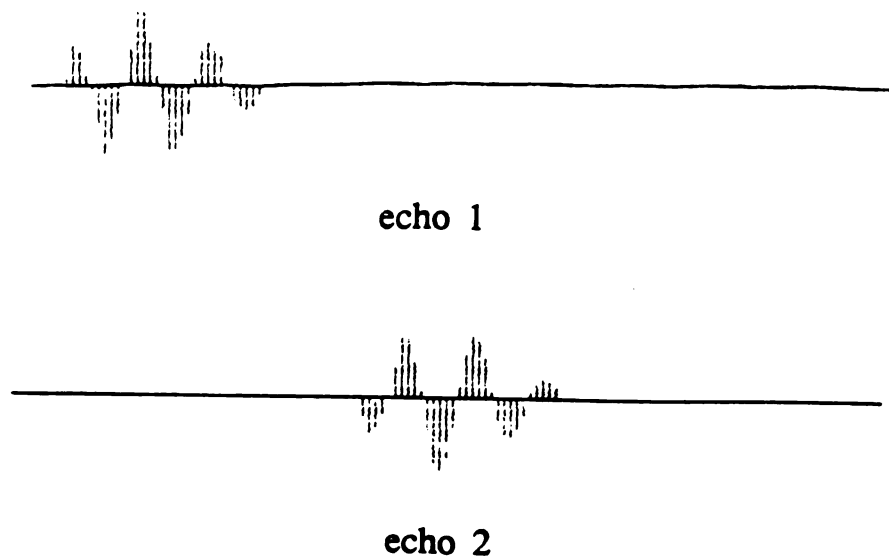


Figure 3.3.4 Reflected signal from test object 1

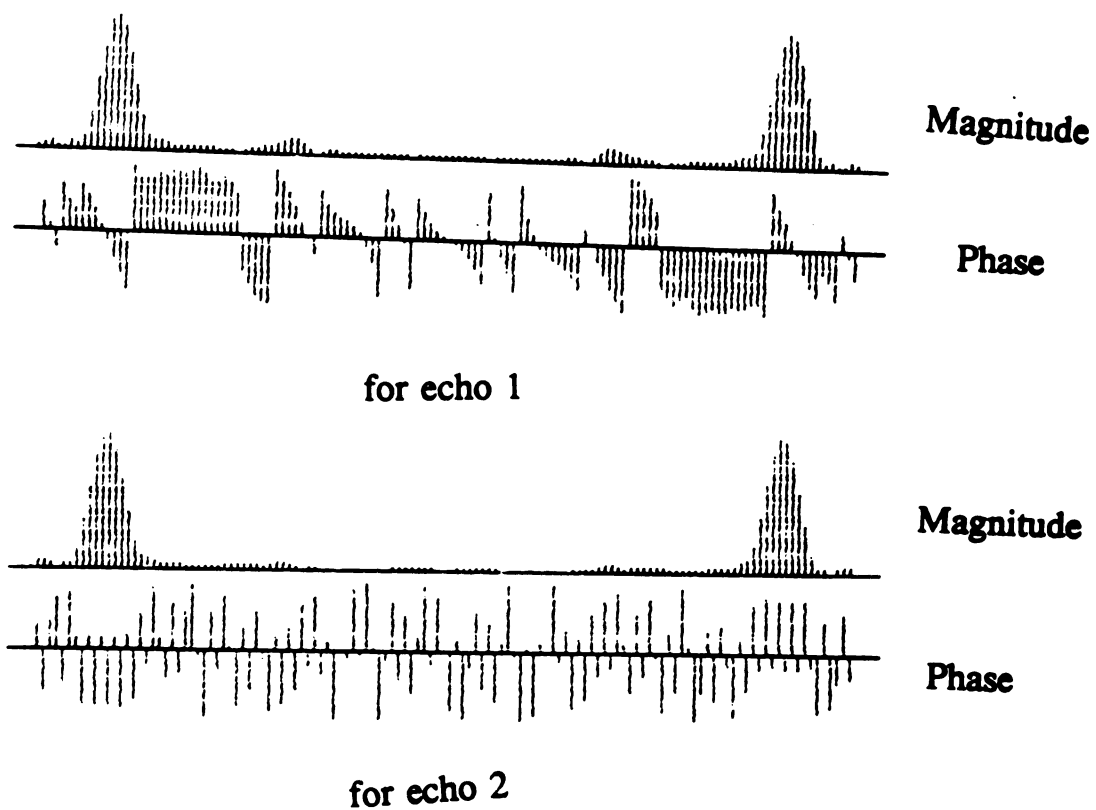
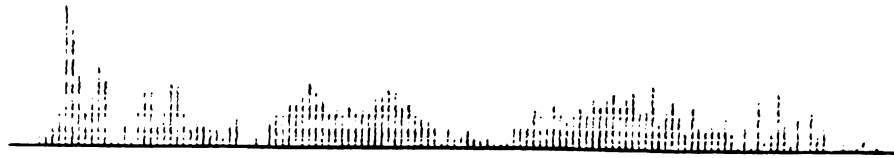
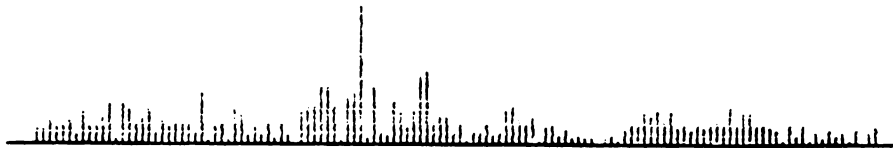


Figure 3.3.5 Frequency spectrum of the reflected signal



for echo 1



for echo 2

Figure 3.3.6 Impulse response function in test 1

Using two the calculation techniques described previously, the result obtained from the impulse response is given in Table 3.3.1, the result from the ratios of the signal magnitude, the ratio of the peak values and the ratio of the magnitude summation, are shown in Table 3.3.2 and Table 3.3.3.

3.3.2 Result for the Uni-directional Attenuation Determination from Known Incident Signal

The model used for this experiment is shown in Figure 3.3.7. The experimental procedure was outlined in subsection 3.2.2.

Figures 3.3.8 through 3.3.13 show the sampled signals, their frequency spectrums and the corresponding impulse response functions. The reflection coefficient at the water/plexi glass interface was calculated following the two methods discussed in subsection 3.2.3.

A $12.75cm \times 1.1cm \times 6.35cm$, $109.046g$ sample of the test object was used to calculate the impedance of the test object. The density of the object, ρ_1 , was calculated as:

$$\rho_1 = \frac{109.046g}{92.30cm^3} = 1.18146g/cm^3 = 1181.46kg/m^3 \quad (3.3.1)$$

The velocity of ultrasound in the test material, c_1 , was measured as:

$$c_1 = 2805m/s \quad (3.3.2)$$

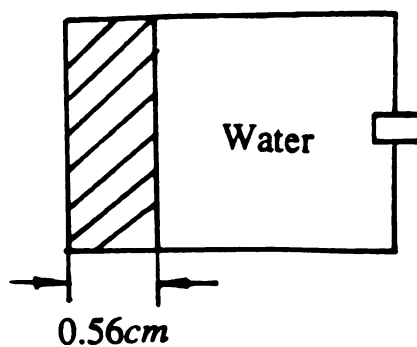


Figure 3.3.7 Test object 2



Figure 3.3.8 Incident signal for test object 2

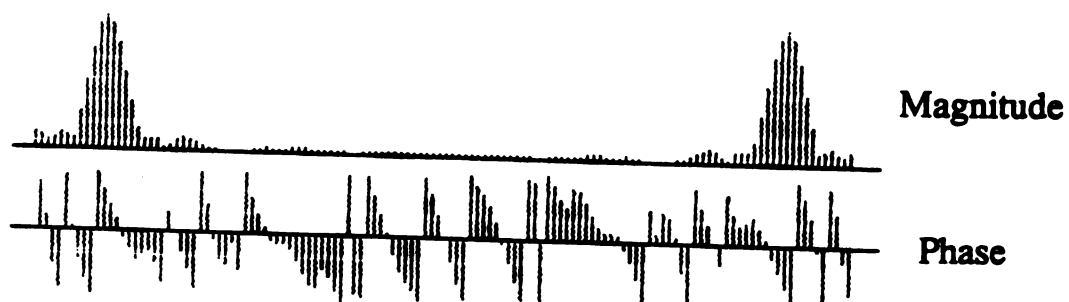
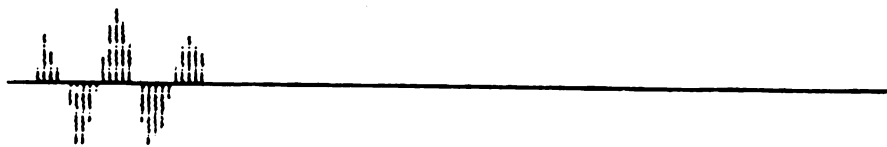


Figure 3.3.9 Frequency spectrum of the incident signal



Figure 3.3.10 Impulse response of the incident signal

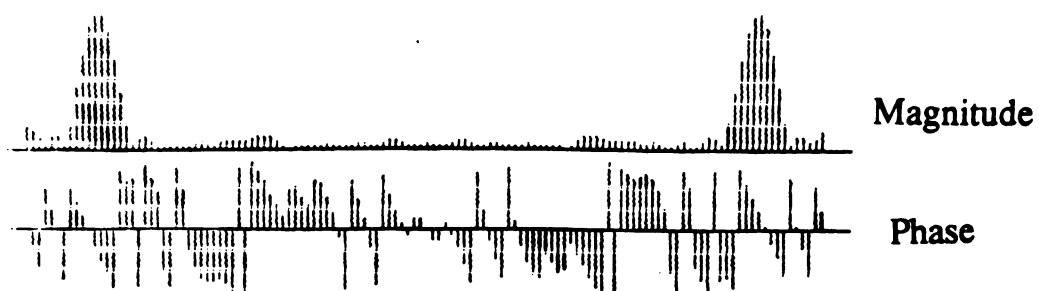


echo 1

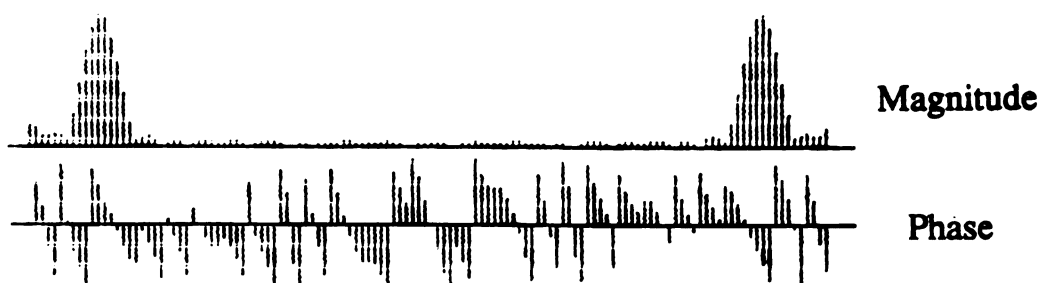


echo 2

Figure 3.3.11 Reflected signal from the plexi glass/air interface

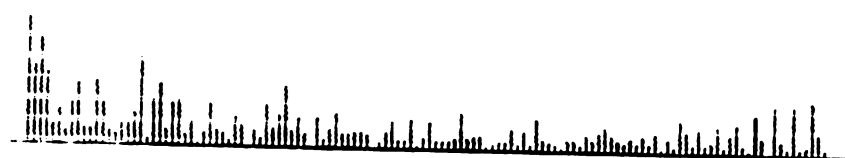


for echo 1

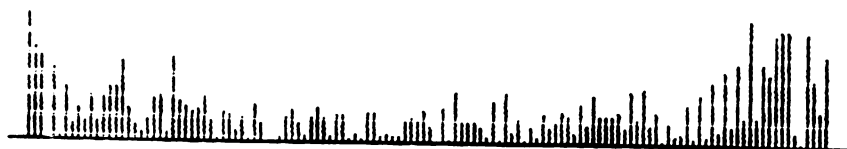


for echo 2

Figure 3.3.12 Frequency spectrum of the reflected signal



for echo 1



for echo 2

Figure 3.3.13 Impulse response in test 2

From equation (3.2.38), the impedance of the plexi glass is given by:

$$Z_1 = \rho_1 c_1 = 1181.46 \text{ kg/m}^3 \times 2805 \text{ m/s} = 3.314 \times 10^6 \text{ kg/m}^2 \text{ s} \quad (3.3.3)$$

The impedance of water (Z_0) was chosen from Table 2.1.2, which is:

$$Z_0 = 1524 \times 10^3 \text{ kg/m}^2 \text{ s} \quad (3.3.4)$$

Following equation (3.2.37), the reflection coefficient at the water/plexi glass interface was determined as:

$$r_1 = \frac{Z_1 - Z_0}{Z_1 + Z_0} = 0.37 \quad (3.3.5)$$

The reflection coefficient was also obtained by using the other method discussed in subsection 3.2.2. From equation (3.2.40),

$$r'_1 = \frac{a_1}{a_0} = \frac{1.088679 \times 10^7}{2.398081 \times 10^7} = 0.45 \quad (3.3.6)$$

where a_1 and a_0 used are the magnitudes of the impulse response functions shown in Figure 3.3.14. and Figure 3.3.11, respectively. These two values of the reflection coefficient were used in the calculations of the attenuation coefficient. The calculation results are tabulated in Table 3.3.4.

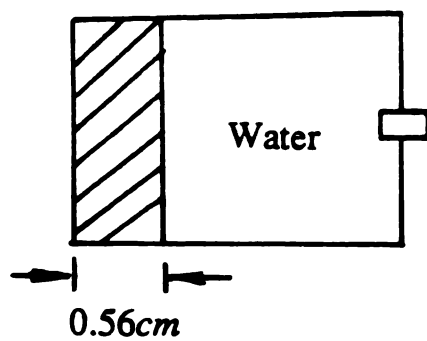
3.3.3 Experimental Result for Uni-directional Attenuation without Knowing the Incident Signal

Two acrylic blocks with different thicknesses were used in this exper-

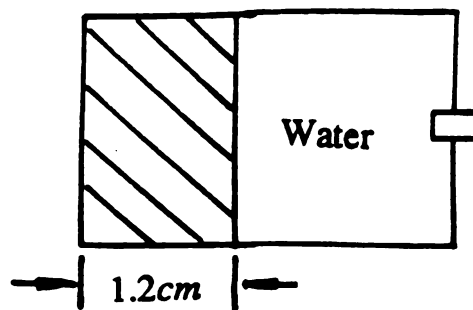
iment. They are shown in Figure 3.3.14. The sampled signals and their frequency spectrum, as well as the corresponding impulse response functions are shown in Figures 3.3.15 through 3.3.23.

The attenuation coefficient was calculated following equation (3.2.44). The impulse response magnitudes and the ratio of the peak values of the reflected signals, as well as the ratio of the magnitude summations were used in the calculation. The results are given in Table 3.3.5.

The analysis of these experimental results, together with the comparison of the simulation data, is given in chapter 4.



Sample 1



Sample 2

Figure 3.3.14 Test object 3

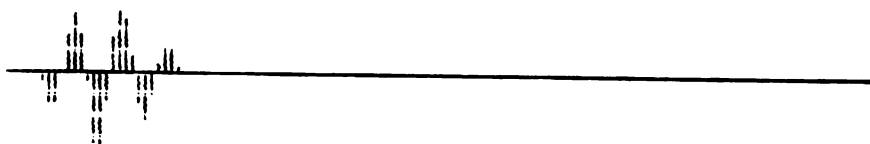


Figure 3.3.15 Incident signal for test 3

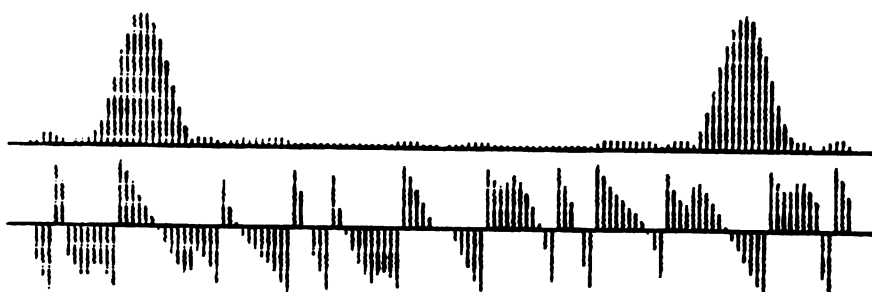


Figure 3.3.16 Frequency spectrum of the incident signal

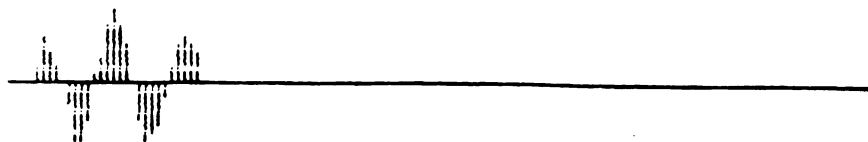


Figure 3.3.17 Reflected signal in sample 1



Figure 3.3.18 Frequency spectrum of the reflected signal in sample 1

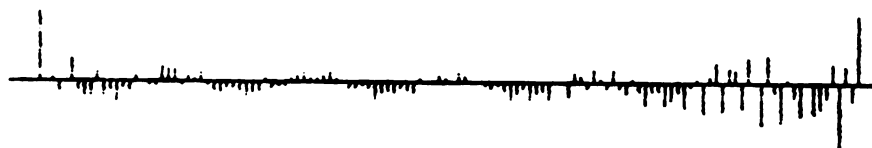


Figure 3.3.19 Impulse response in sample 1

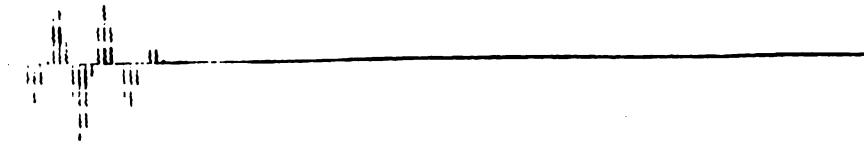


Figure 3.3.20 Reflected signal from sample 2

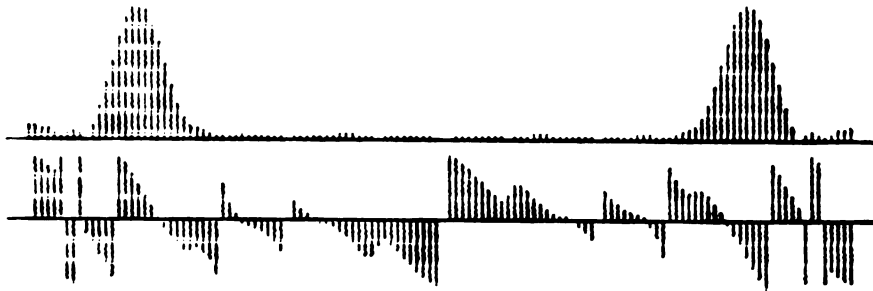


Figure 3.3.21 Frequency spectrum of the reflected signal in sample 2



Figure 3.3.22 Impulse response for sample 2

Table 3.3.1 Result for test object 1
---using the impulse response function

Layer	Reflection coefficient (water/plexiglass)	Attenuation coefficient (cm^{-1})
Plexiglass	0.37	0.75
Plexiglass	0.45	0.68

Table 3.3.2 Result for test object 1
---using the signal peak value

Layer	Reflection coefficient (water/plexiglass)	Attenuation coefficient (cm^{-1})
Plexiglass	0.37	0.40
Plexiglass	0.45	0.33

Table 3.3.3 Result for test object 1
---using the signal magnitude sum

Layer	Reflection coefficient (water/plexiglass)	Attenuation coefficient (cm^{-1})
Plexiglass	0.37	0.37
Plexiglass	0.45	0.30

Table 3.3.4 Result for test object 2

Layer	Reflection coefficient (water/plexiglass)	Attenuation coefficient (cm^{-1})
Plexiglass	0.37	0.63
Plexiglass	0.45	0.56

Table 3.3.5 Result for test object 3

Data type	Attenuation coefficient(cm^{-1})
Impulse response	0.58
Signal sum	0.45
Signal peak value	0.44

Chapter 4

Analysis of Experimental Results

The experimental results obtained in chapter 3 are compared with simulation data in this chapter. The validity of the measurement techniques is discussed. In section 4.1, the experimental data from the impulse response function are analyzed, along with the simulation results. In section 4.2, the consistency of the two attenuation calculation methods is discussed, based on the simulation data and the experimental results obtained in section 3.3.

4.1 Tradeoffs for Finding the Impulse Response Function

The attenuation measurement method introduced in section 2.3 depends heavily on the ability to determine the impulse response function accurately. Theoretically, the impulse response function is a train of impulses, each impulse corresponds to each boundary inside the test material. In practice, however, it is not always the case. Noise may be introduced in the A/D conversion. The finite frequency band of the FFT may cause computation errors. The division operation in deconvolution can even enlarge the effect of those errors. The experimental results in chapter 3 show that even the noises in the impulse response function do

not distort the impulses in shape, they already affect the magnitudes of the impulses.

It is worthwhile to know the limitation of the deconvolution technique for the ultrasound attenuation determination. This was done by simulation. The synthetic ultrasound signals used in the simulation were made close to the actual signals in signal intensity and frequency. Figures 4.1.1 shows the simulation result. As comparison of this result, Figures 4.1.2 shows the measured data and result. From the simulation result, it is clear that the deconvolution technique and the FFT algorithm used in this study are qualified for the attenuation measurement. It turns out the sampled signals need to be processed in order to improve the impulse response function.

Two signal processing methods were investigated. They are: 1) interpolation of the sampled signals; 2) correlation to obtain impulse response function.

1) Interpolation of the sampled signals

The sampled values of the signals were interpolated by inserting the mean value of two adjoining samples to the middle of these samples. The simulation result without using the interpolation is shown in Figure 4.1.3, as a comparison with the result obtained from the interpolation shown in

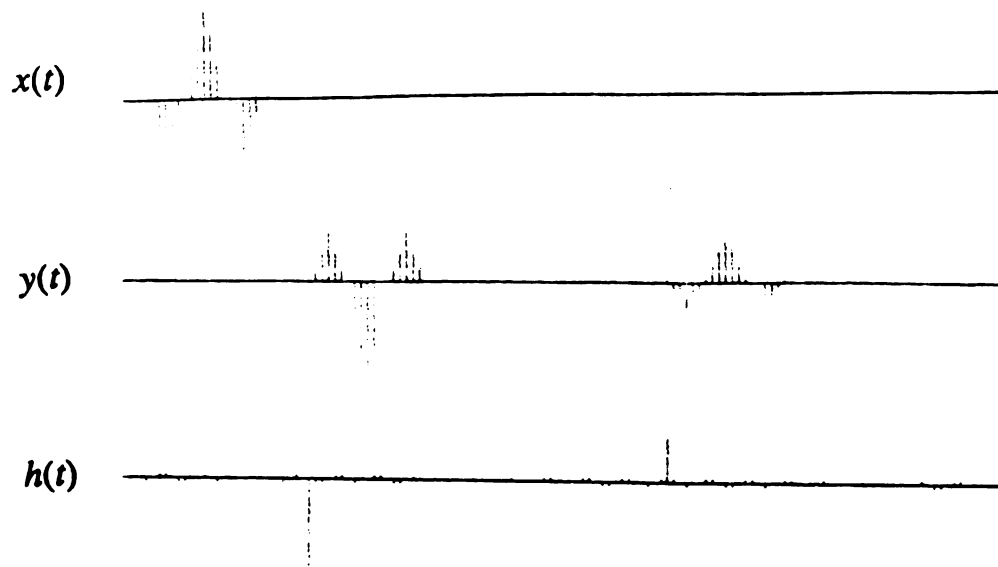


Figure 4.1.1 Simulation result

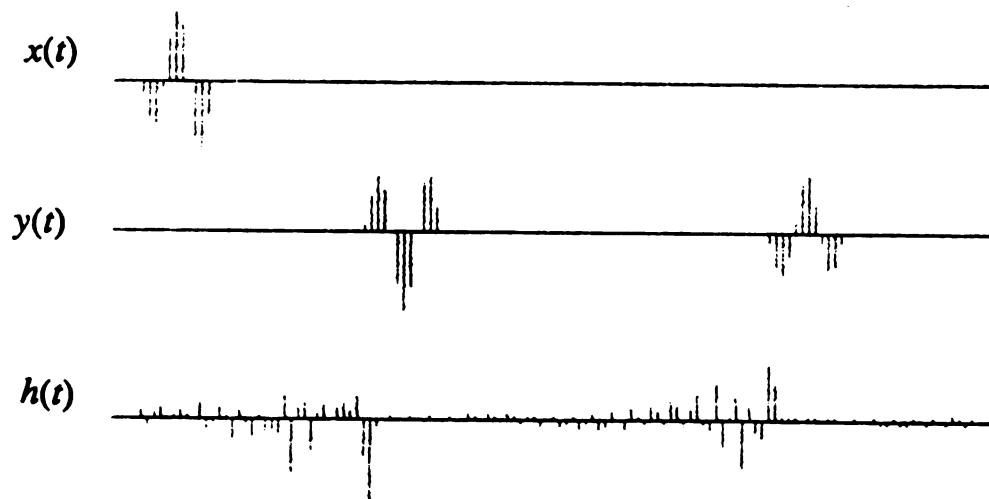


Figure 4.1.2 Measured result

Figure 4.1.4. The results for the actual signals are shown in Figures 4.1.5 and 4.1.6.

These results show the interpolation can improve the impulse response function. For this was a preliminary study of the interpolation effect, only the simple interpolation algorithm was investigated. Other interpolation algorithms may give better results.

2) Correlation to obtain impulse response function The auto-correlation of incident signal and the cross-correlation of the incident and reflected signals can be used to determine the impulse response function. This is derived as follows.

Assume:

$x(t)$ = incident signal

$X(f)$ = frequency spectrum of the incident signal

$X^*(f)$ = complex conjugate of $X(f)$

$y(t)$ = reflected signal

$Y(f)$ = frequency spectrum of the reflected signal

$Y^*(f)$ = complex conjugate of $Y(f)$

$r_{xx}(t)$ = auto-correlation of $x(t)$

$r_{xy}(t)$ = cross-correlation of $x(t)$ and $y(t)$

$R_{xx}(f)$ = frequency spectrum of $r_{xx}(t)$



Figure 4.1.3 Simulation result without the interpolation

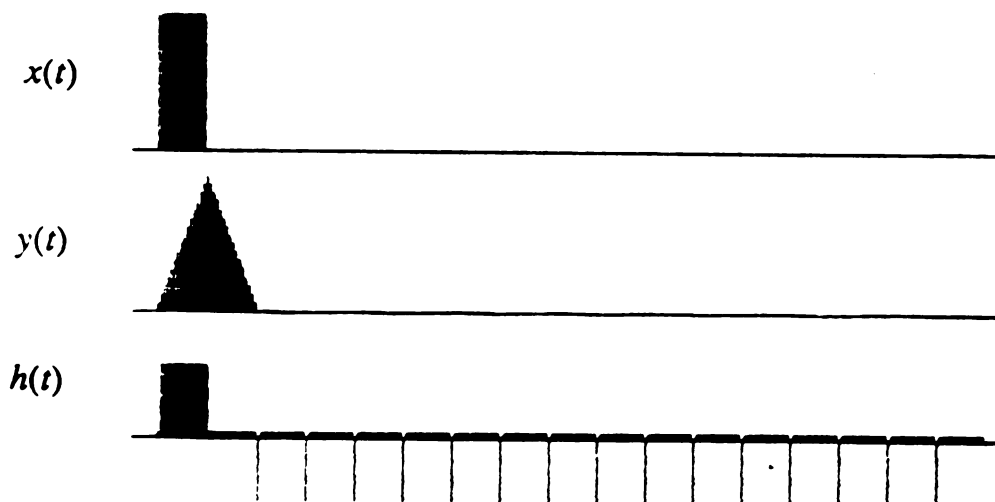


Figure 4.1.4 Simulation result with the interpolation

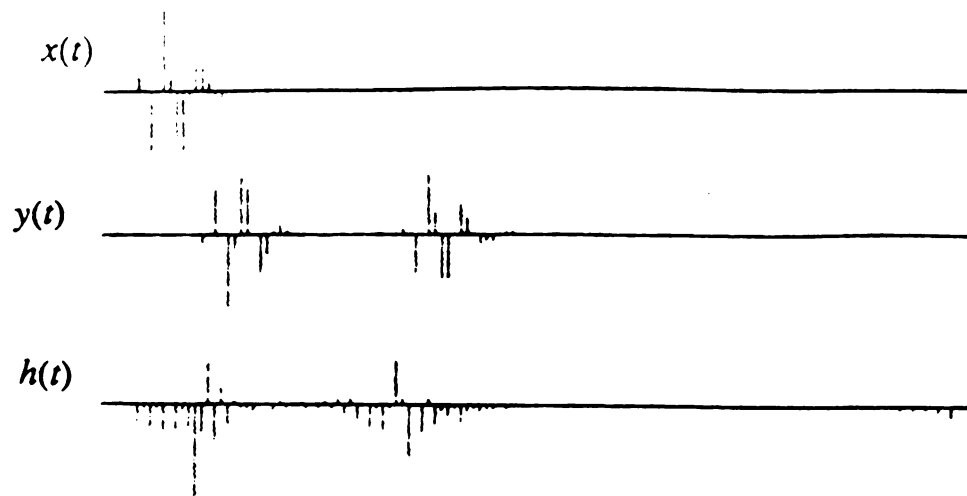


Figure 4.1.5 Measured result without the interpolation

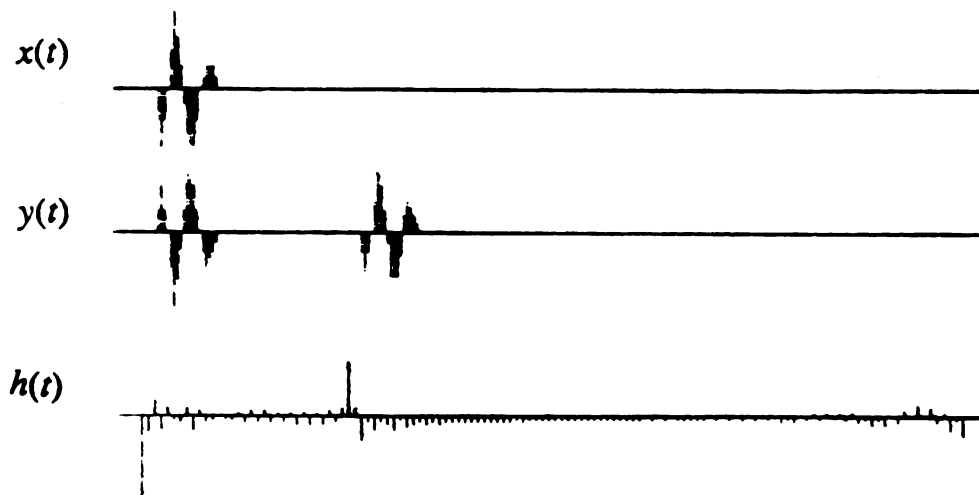


Figure 4.1.6 Measured result with the interpolation

$R_{xy}(f)$ = frequency spectrum of $r_{xy}(t)$

$h(t)$ = impulse response

$H(f)$ = frequency spectrum of $h(t)$

From the correlation properties,

$$R_{xx}(f) = X(f)X^*(f) \quad (4.1.1)$$

$$R_{xy}(f) = X(f)Y^*(f) = X^*(f)Y(f) \quad (4.1.2)$$

The frequency spectrum of the impulse response function is given by:

$$\frac{R_{xy}(f)}{R_{xx}(f)} = \frac{X^*(f)Y(f)}{X^*(f)Y(f)} = \frac{Y(f)}{X(f)} = H(f) \quad (4.1.3)$$

Thus,

$$h(t) = F^{-1}(H(f)) \quad (4.1.4)$$

where $F^{-1}()$ is the inverse Fourier transform operator.

In the experiment, the incident signal and the reflected signal were processed following the procedure shown above. The result for the actual signals are shown in Figures 4.1.7. It is seen that the improvement by this technique is fairly limited.

4.2 Discussion

In section 2.4, it was theoretically shown that the ratio of the signal magnitudes can replace the ratio of the impulse response for the determination of the acoustic attenuation. A critical issue upon the validity of this

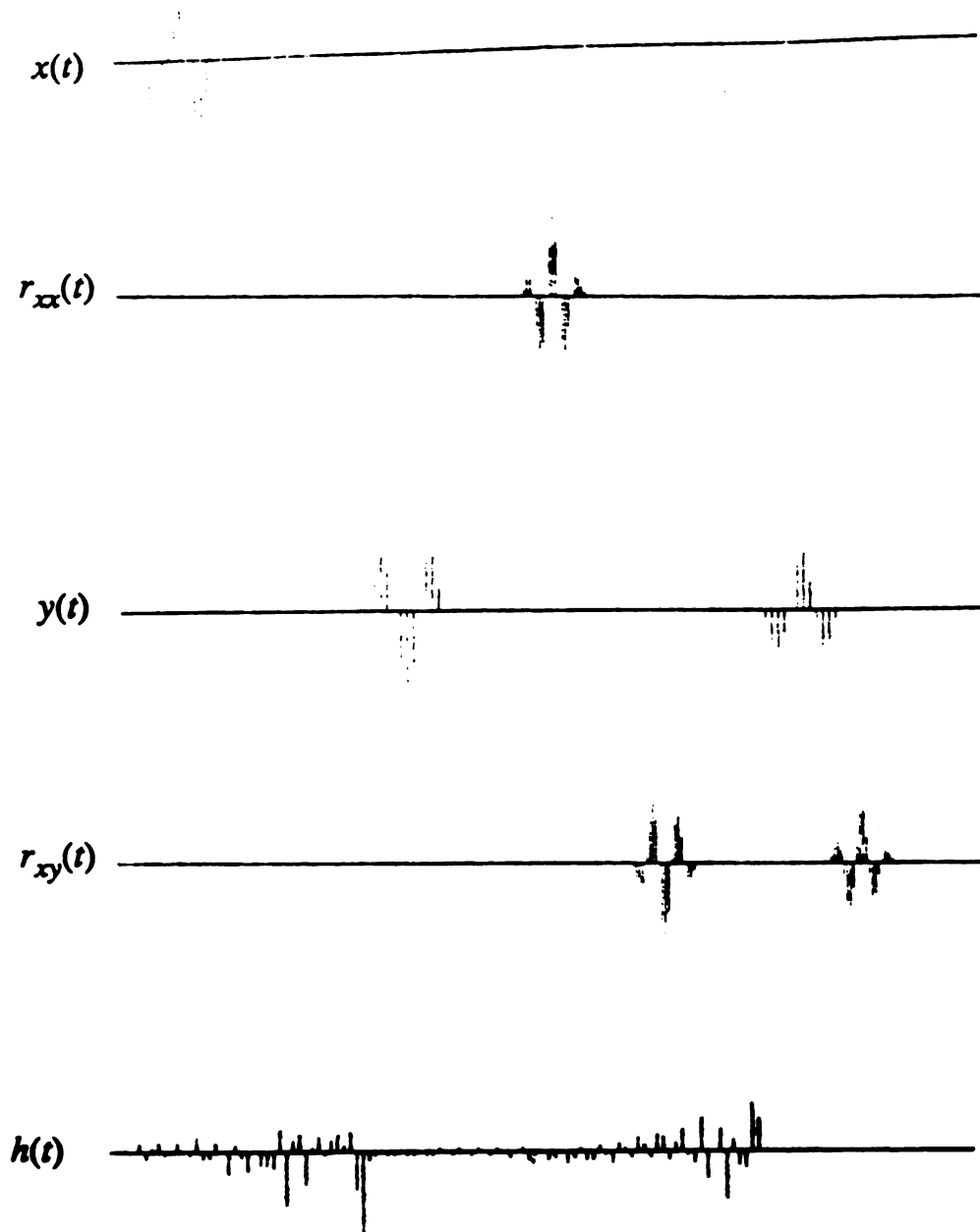


Figure 4.1.7 Measured result using correlation

method is the consistency of the two ratios in practical environment. A verification of the consistency was done by synthetic signals.

The verification is straight forward: for each set of synthetic signals, the corresponding impulse response functions are calculated by deconvolution. Then the ratio of the impulses are compared with the ratio of the signal magnitudes. Figure 4.2.1 and Table 4.2.1 show the result for the first set of data. Figure 4.2.2 and Table 4.2.2 show the case for the second set of data. For the estimate of the signal magnitude ratio, both the peak values and the magnitude summation were used.

In Tables 4.2.1 and 4.2.2, the ratio of the impulses and the ratio of the signal magnitudes are identical, which is consistent with the theoretical result.

The experimental results in chapter 3, however, are not so consistent. The reasons are the following. The first reason is that the impulse response functions do not consist of only the pure impulses. Thus the magnitudes of the impulses used in the calculation can be different from the "true" magnitudes. For a poor impulse response (Figure 3.3.6), the difference between the two calculation results is large (Tables 3.3.1, 3.3.2, 3.3.3). For a better impulse function (Figures 3.3.19 and 3.3.22), the difference becomes much smaller. In addition, the large variation of the

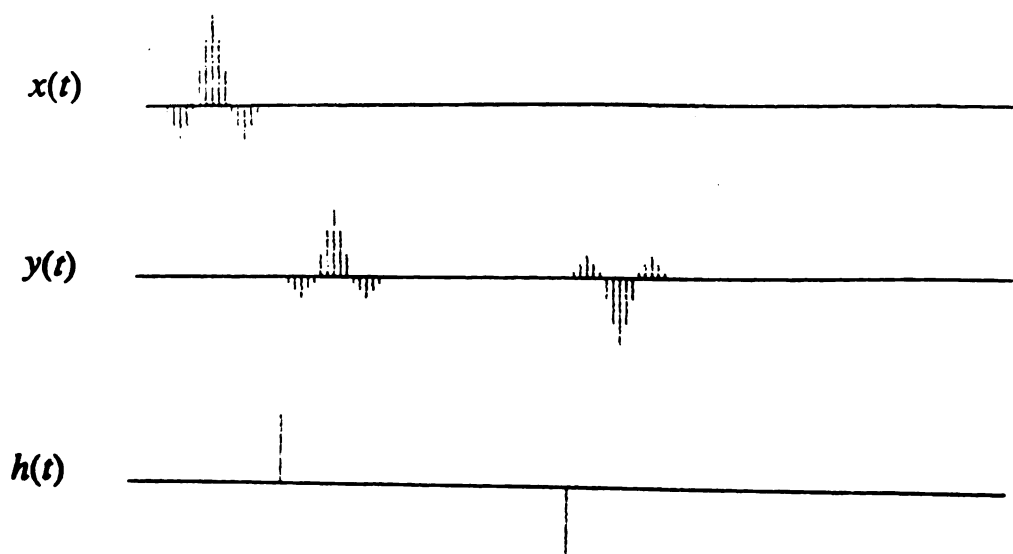


Figure 4.2.1 Simulation data 1

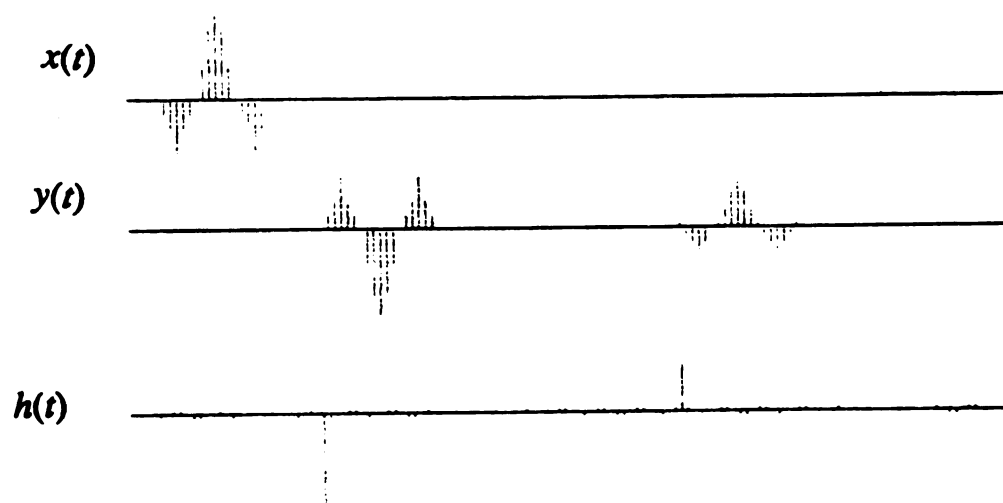


Figure 4.2.2 Simulation data 2

Table 4.2.1 Ratios for simulation data 1

Impulse response	Signal magnitude sum	Signal peak value
1.000	1.000	1.000

Table 4.2.2 Ratios for simulation data 2

Impulse response	Signal magnitude sum	Signal peak value
1.937	2.451	2.000

ratios of the impulses in the three experiments indicate the poor accuracy of those ratios.

As pointed in chapter 3, the third experiment setup is the most accurate one. The results in that experiment are indeed much more consistent than the other two. Hence the result of the third experiment can be considered as the most accurate one. A important observation is that in all the experiments, the results obtained from the signal magnitude ratios are much closer to the result in the third experiment, in comparison of the results from the impulse response function.

From these discussions, it is clear that the signal magnitude ratio is more accurate than the ratio of the impulse response, in general.

4.3 Conclusion and Suggestion for Future Study

This thesis has developed two methods that can extract both the variation of attenuation coefficient and the variation of reflection coefficient along the path of propagation. The corresponding impedance profile can be easily calculated from the reflection coefficient (equation (3.2.12, 3.2.34)). The variation of impedance obtained by these techniques should be more accurate than that by the ultrasonic impediography methods, since the latter neglect the attenuation in the medium, whereas the

methods outlined in this thesis take into account the ultrasonic attenuation along the path of propagation. In fact, the development of imaging techniques utilizing the attenuation coefficient is the main thrust of the research reported here.

Between the two methods presented in this thesis, the one utilizing the ratio of the reflected signals is more favorable for imaging applications, because of its simplicity and accuracy. This method depends heavily on the ability to accurately obtain the reflected signals accuracy, it introduces other problems such as noise contamination and signal dispersion. The attenuation coefficient for biological matter has been found to be frequency dispersive so that a large bandwidth may result in nonuniform attenuation of different frequency components.

There are several approaches that could improve the accuracy of attenuation calculation's evaluation. One is to explore different schemes to determine the ratio of the reflected signals. Two methods were outlined to obtain this signal ratio. However, further development may be desirable since the accuracy of the ratio plays a critical role in the method. Another way to improve accuracy may be to apply sophisticated signal processing techniques. In the work reported here, a chebyshev filter was employed which worked well for the test models investigated. As the thickness of the test object increases, the power and hence the signal to noise ratio

decreases for reflected echoes from the deep lying boundaries in the object. In that case, other signal processing schemes may be necessary to improve the signal to noise conditions.

Bibliography

1. Beretsky, I., Farrell, G.A., *Improvement of Ultrasonic Imaging and Media Characterization by Frequency Domain Deconvolution, Experimental Study with Non-Biological Models*, Ultrasound in Medicine, Vol. 3B, 1977
2. Giesey, J.J., *Automated System for Determining the Acoustic Impulse Response of a Layered Model*, M.S. Thesis, Michigan State University, 1986
3. Ho, B., Jayasumana, A., Fang, C.G., *Ultrasonic Attenuation Tomography by Dual Reflection Technique*, Ultrasonics Symposium, 770, 1983
4. Jayasumana, M.A.A.P., *Acoustic Attenuation and Impedance Characterization by Bi-Directional Impulse Response Technique*, M.S. Thesis, Michigan State University, 1982
5. Jonse, J.P., *Ultrasonic impediography and Its Application to Tissue Characterization*, Recent Advances in Ultrasound in Biomedicine, 1977
6. Kuc, R., Schwartz, M., Kaufman, J., *Kalman Filtering Approach in the Analysis of Reflected Ultrasonic Signal*, 4 th International Symposium on Ultrasonic Imaging and Tissue Characterization, N.B.S., 1979
7. Papoulis, A., Chamas, C., *Improvement at Range Resolution by Spectral Extrapolation*, 4 th International Symposium on Ultrasonic Imaging and Tissue Characterization, N.B.S., 1979
8. Stewart, H.F., Stratmeyer, M.E., *An Overview of Ultrasound: Theory, Measurement, Medical Applications, and Biological Effects*, U.S. Department of Health and Human Services, July, 1982
9. Wells, P.N.T., *Physical Principles of Ultrasonic Diagnosis*, Academic Press, 1969

MICHIGAN STATE UNIV. LIBRARIES



31293006952695